# NASA Tech Briefs

National Aeronautics and
Space Administration

**Electronic Components and Circuits**

**Electronic Systems**

**Physical Sciences**

**Materials**

**Computer Programs**

**Mechanics**

**Machinery**

**Fabrication Technology**

**Mathematics and Information Sciences**

**Life Sciences**

# INTRODUCTION

Tech Briefs are short announcements of innovations originating from research and development activities of the National Aeronautics and Space Administration. They emphasize information considered likely to be transferable across industrial, regional, or disciplinary lines and are issued to encourage commercial application.

## Availability of NASA Tech Briefs and TSPs

Requests for individual Tech Briefs or for Technical Support Packages (TSPs) announced herein should be addressed to

**National Technology Transfer Center**
Telephone No. **(800) 678-6882** or via World WIde Web at **www2.nttc.edu/leads/**

Please reference the control numbers appearing at the end of each Tech Brief. Information on NASA's Commercial Technology Team, its documents, and services is also available at the same facility or on the World Wide Web at **www.nctn.hq.nasa.gov**.

Commercial Technology Offices and Patent Counsels are located at NASA field centers to provide technology-transfer access to industrial users. Inquiries can be made by contacting NASA field centers and program offices listed below.

# NASA Field Centers and Program Offices

**Ames Research Center**
*Carolina Blake*
*(650) 604-1754 or*
*cblake@mail.arc.nasa.gov*

**Dryden Flight Research Center**
*Jenny Baer-Riedhart*
*(661) 276-3689 or*
*jenny.baer-riedhart@dfrc.nasa.gov*

**Goddard Space Flight Center**
*Nona Cheeks*
*(301) 286-5810 or*
*nona.k.cheeks@gsfc.nasa.gov*

**Jet Propulsion Laboratory**
*Merle McKenzie*
*(818) 354-2577 or*
*merle.mckenzie@jpl.nasa.gov*

**Johnson Space Center**
*Charlene E. Gilbert*
*(281) 483-3809 or*
*commercialization@jsc.nasa.gov*

**John F. Kennedy Space Center**
*Jim Aliberti*
*(321) 867-6224 or*
*Jim.Aliberti-1@ksc.nasa.gov*

**Langley Research Center**
*Sam Morello*
*(757) 864-6005 or*
*s.a.morello@larc.nasa.gov*

**Glenn Research Center**
*Larry Viterna*
*(216) 433-3484 or*
*cto@grc.nasa.gov*

**George C. Marshall Space Flight Center**
*Vernotto McMillan*
*(256) 544-2615 or*
*vernotto.mcmillan@msfc.nasa.gov*

**John C. Stennis Space Center**
*Kirk Sharp*
*(228) 688-1929 or*
*technology@ssc.nasa.gov*

**NASA Program Offices**
At NASA Headquarters there are seven major program offices that develop and oversee technology projects of potential interest to industry:

**Carl Ray**
*Small Business Innovation Research Program (SBIR) & Small Business Technology Transfer Program (STTR)*
*(202) 358-4652 or*
*cray@mail.hq.nasa.gov*

**Dr. Robert Norwood**
*Office of Commercial Technology (Code RW)*
*(202) 358-2320 or*
*rnorwood@mail.hq.nasa.gov*

**John Mankins**
*Office of Space Flight (Code MP)*
*(202) 358-4659 or*
*jmankins@mail.hq.nasa.gov*

**Terry Hertz**
*Office of Aero-Space Technology (Code RS)*
*(202) 358-4636 or*
*thertz@mail.hq.nasa.gov*

**Glen Mucklow**
*Office of Space Sciences (Code SM)*
*(202) 358-2235 or*
*gmucklow@mail.hq.nasa.gov*

**Roger Crouch**
*Office of Microgravity Science Applications (Code U)*
*(202) 358-0689 or*
*rcrouch@hq.nasa.gov*

**Granville Paules**
*Office of Mission to Planet Earth (Code Y)*
*(202) 358-0706 or*
*gpaules@mtpe.hq.nasa.gov*

TechBriefs

National Aeronautics and
Space Administration

January 2003
03-01

5 **Electronic Components and Circuits**

13 **Electronic Systems**

19 **Physical Sciences**

29 **Materials**

33 **Computer Programs**

37 **Mechanics**

43 **Machinery**

47 **Fabrication Technology**

53 **Mathematics and Information Sciences**

59 **Life Sciences**

# Electronic Components and Circuits

## Hardware, Techniques, and Processes


7 Optoelectronic Tool Adds Scale Marks to Photographic Images
8 Compact Interconnection Networks Based on Quantum Dots
10 Laterally Coupled Quantum-Dot Distributed-Feedback Lasers
10 Bit-Serial Adder Based on Quantum Dots

# Optoelectronic Tool Adds Scale Marks to Photographic Images

Scale marks are optically projected into any desired scene.

*John F. Kennedy Space Center, Florida*

A simple, easy-to-use optoelectronic tool projects scale marks that become incorporated into photographic images (including film and electronic images). The sizes of objects depicted in the images can readily be measured by reference to the scale marks. The role played by the scale marks projected by this tool is the same as that of the scale marks on a ruler placed in a scene for the purpose of establishing a length scale. However, this tool offers the advantage that it can put scale marks quickly and safely in any visible location, including a location in which placement of a ruler would be difficult, unsafe, or time-consuming.

The tool (see Figure 1) includes an aluminum housing, within which are mounted four laser diodes that operate at a wavelength of 670 nm. The laser diodes are spaced 1 in. (2.54 cm) apart along a baseline. The laser diodes are mounted with setscrews, which are used to adjust their beams to make them all parallel to each other and perpendicular to the baseline. During the adjustment process, the effect of the adjustments is observed by measuring the positions of the laser-beam spots on a target 80 ft (≈24 m) away. Once the adjustments have been completed, the laser beams define three 1-in. (2.54-cm) intervals and the location of each beam is defined to within 1/16 in. (≈1.6 mm) at any target distance out to about 80 ft (≈24 m).

The distance between the laser-beam spots as seen in an image is strictly defined only along an axis parallel to the baseline and perpendicular to the laser beam (also perpendicular to the line of sight of the camera, assuming that the camera-to-target distance is much greater than the distance between the tool and the camera lens). If a flat target surface illuminated by the laser beams is tilted with respect to the aforesaid axis, then the distance along the target surface between scale marks is proportional to the secant of the tilt angle. If one knows the tilt angle, one can correct for it. Even if one does not know the tilt angle precisely, it may not matter: For example, at a tilt of 10°, the secant is approximately 1.0154, so that the tilt error is only about 1.54 percent, which is negligibly small for a typical application in which only approximate measurements are needed.

Each diode laser generates a light beam having a power of 3 mW and consumes an input power of 150 mW. The laser diodes are powered by a lithium cell that can sustain operation for an interval of an hour or more. Because the optical performances of the laser diodes are equivalent to those of most laser-based auditorium pointers, the use of the tool should not pose a major con-

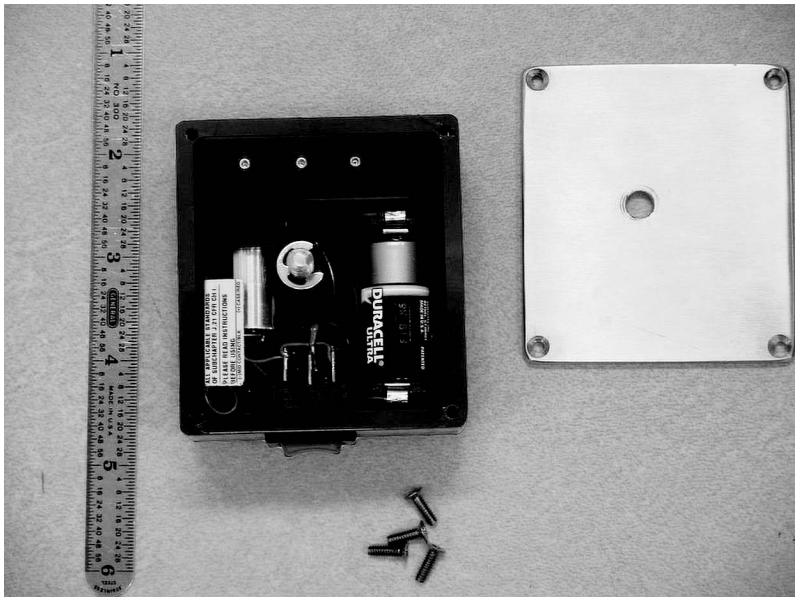


**TOOL WITH COVER REMOVED**

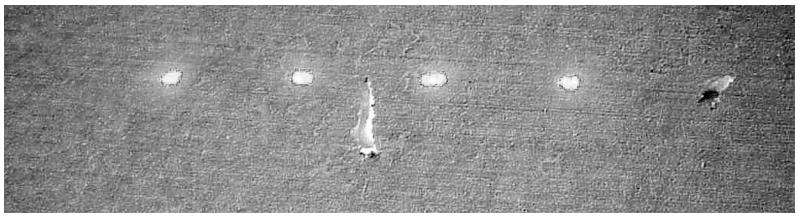

**LIGHT SPOTS PROJECTED BY THE TOOL ONTO A SURFACE TO BE INSPECTED**

Figure 1. The **Tool Contains Four Laser Diodes** that generate evenly spaced parallel beams that project light spots onto an object to be photographed for inspection. The laser diodes are located in the curved tubes that protrude from the rest of the housing.

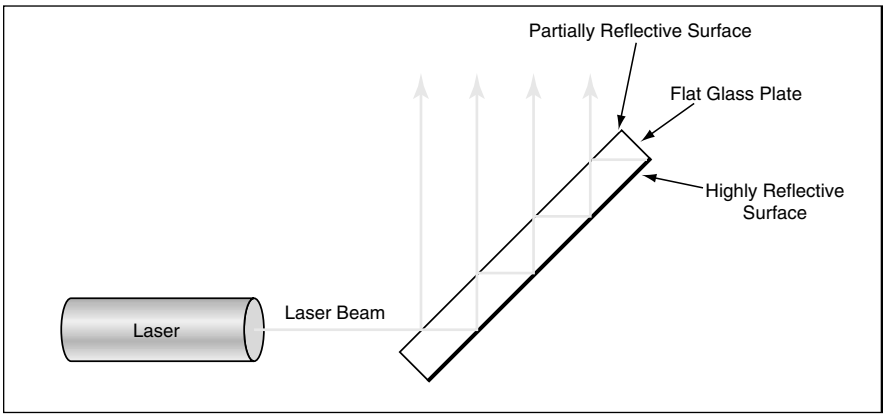


Figure 2. A **Laser Beam Would Be Split** into four parallel beams in this simple optical assembly. The four beams would not be of equal power, but in many applications, this inequality would not be a great disadvantage.

cern for eye safety — provided, of course, that one observes the usual precaution of not looking directly into the laser beams.

The tool can readily be attached to almost any camera by use of the standard tripod nut on the underside of the camera. Once the tool is thus attached and properly aligned, it projects the laser scale marks wherever the camera is aimed.

The basic principle of operation of this tool is amenable to a number of potential variations of its design. For example, the number of laser beams could be different from four. For another example, one of the laser beams could be aimed at a known angle relative to the others so that the different distances between laser-beam spots in an image can be used to estimate the distance between the camera/tool combination and the target.

For yet another example, one could reduce the cost of the tool by using a single laser in conjunction with a non-optimum inexpensive simple beam-splitting device to generate all four beams. In this case (see Figure 2), the beam-splitting device would be a flat glass plate coated to be partially reflective on one surface and highly reflective on the other surface. Because the parallelism of the output laser beams would depend only on the parallelism of the glass surfaces and the distance between successive beams would depend only the thickness of the glass surfaces and would vary uncritically with the tilt of the plate, this design would offer the advantage of simplification of alignment. The one shortcoming of this design is that the four laser beams would not be of equal power.

*This work was done by Charlie Stevenson, Jorge Rivera, and Robert Youngquist of* **Kennedy Space Center** *and Robert Cox and William Haskell of Dynacs, Inc. For further information, contact the Kennedy Space Center Technology Commercialization Office at (321) 867-8130. KSC-12201*

## Compact Interconnection Networks Based on Quantum Dots

These networks would exploit the crossing of coplanar signal paths.

*NASA's Jet Propulsion Laboratory, Pasadena, California*

Architectures that would exploit the distinct characteristics of quantum-dot cellular automata (QCA) have been proposed for digital communication networks that connect advanced digital computing circuits. In comparison with networks of wires in conventional very-large-scale integrated (VLSI) circuitry, the networks according to the proposed architectures would be more compact. The proposed architectures would make it possible to implement complex interconnection schemes that are required for some advanced parallel-computing algorithms and that are difficult (and in many cases impractical) to implement in VLSI circuitry.

The difficulty of implementation in VLSI and the major potential advantage afforded by QCA were described previously in "Implementing Permutation Matrices by Use of Quantum Dots" (NPO-20801), *NASA Tech Briefs*, Vol. 25, No. 10 (October 2001), page 42. To recapitulate: Wherever two wires in a conventional VLSI circuit cross each other and are required not to be in electrical contact with each other, there must be a layer of electrical insulation between them. This, in turn, makes it necessary to resort to a noncoplanar and possibly a multilayer design, which can be complex, expensive, and even impractical. As a result, much of the cost of designing VLSI circuits is associated with minimization of data routing and assignment of layers to minimize crossing of wires. Heretofore, these considerations have impeded the development of VLSI circuitry to implement complex, advanced interconnection schemes.

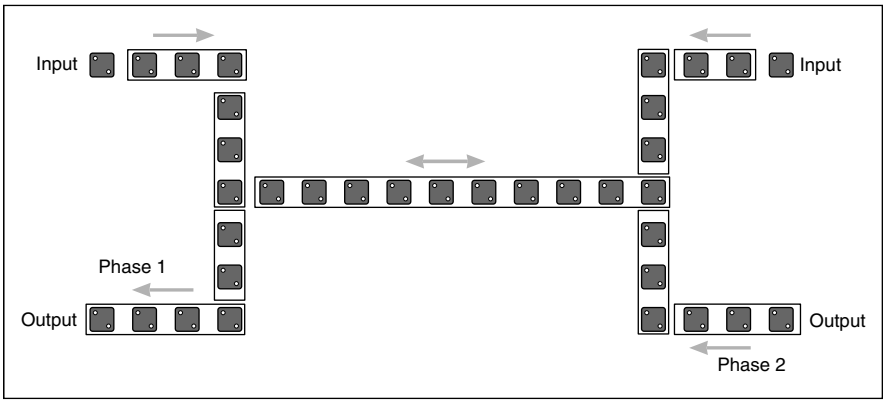


Figure 1. A **QCA-Based Wire for Bidirectional Communication** would be terminated in input and output branches at both ends.

On the other hand, with suitable design and under suitable operating conditions, QCA-based signal paths can be allowed to cross each other in the same plane without adverse effect. In principle, this characteristic could be exploited to design compact, coplanar, simple (relative to VLSI) QCA-based networks to implement complex, advanced interconnection schemes.

The proposed architectures require two advances in QCA-based circuitry beyond basic QCA-based binary-signal wires described in the cited prior article. One of these advances would be the development of QCA-based wires capable of bidirectional transmission of signals. The other advance would be the development of QCA circuits capable of high-impedance state outputs. The high-impedance states would be utilized along with the 0- and 1-state outputs of QCA.

A QCA-based wire for bidirectional communication (see Figure 1) would be terminated in two branches at each end — one branch for input, the other for output. To enable binary signals to propagate both from the left input to the right output terminal and from the right input to the left output terminal, it would be necessary to apply suitably phased clock signals (bias voltages) to QCA subarrays at various positions along the main wire and the end branches. (For complex reasons that must be omitted from this article for lack of space, such clocking is needed in any event to prevent spurious outputs. Here, the clocking would be exploited for the additional purpose of bidirectional communication.)

One especially useful interconnection network is an $N \times N$ crossbar network. A QCA circuit capable of a high-impedance output state would be needed to implement a crosspoint switch in a crossbar network. This is because while all $N$ input

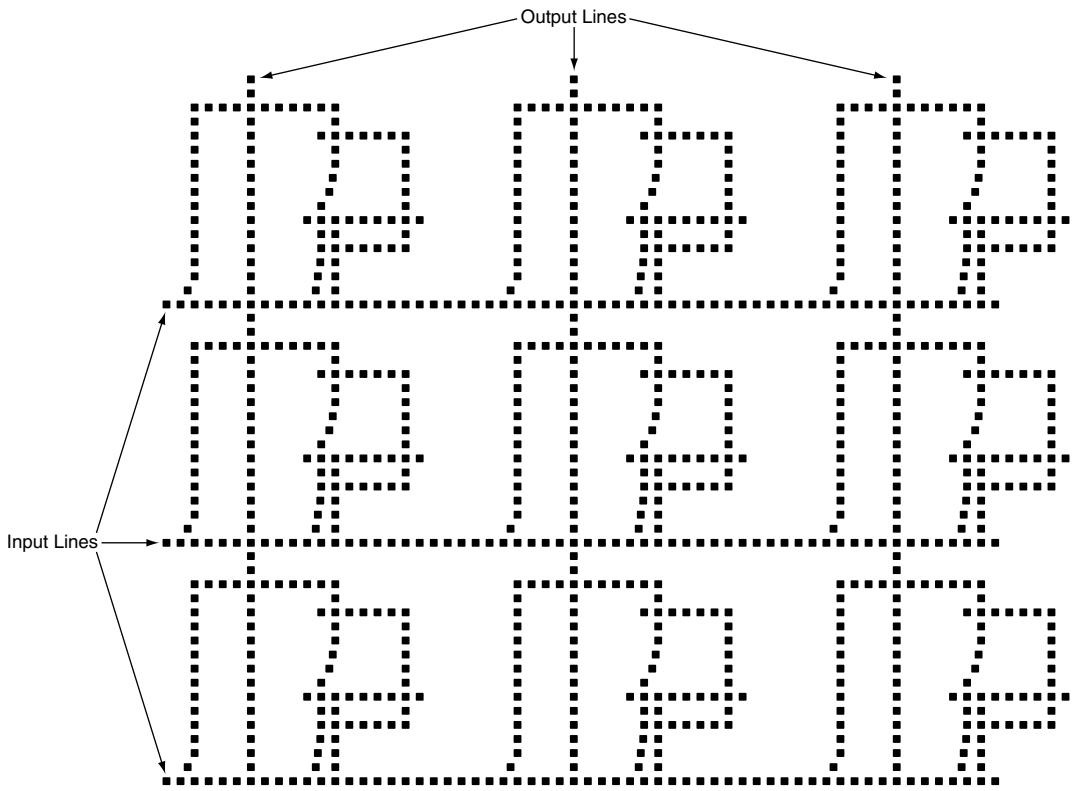


**3×3 CROSSBAR NETWORK**

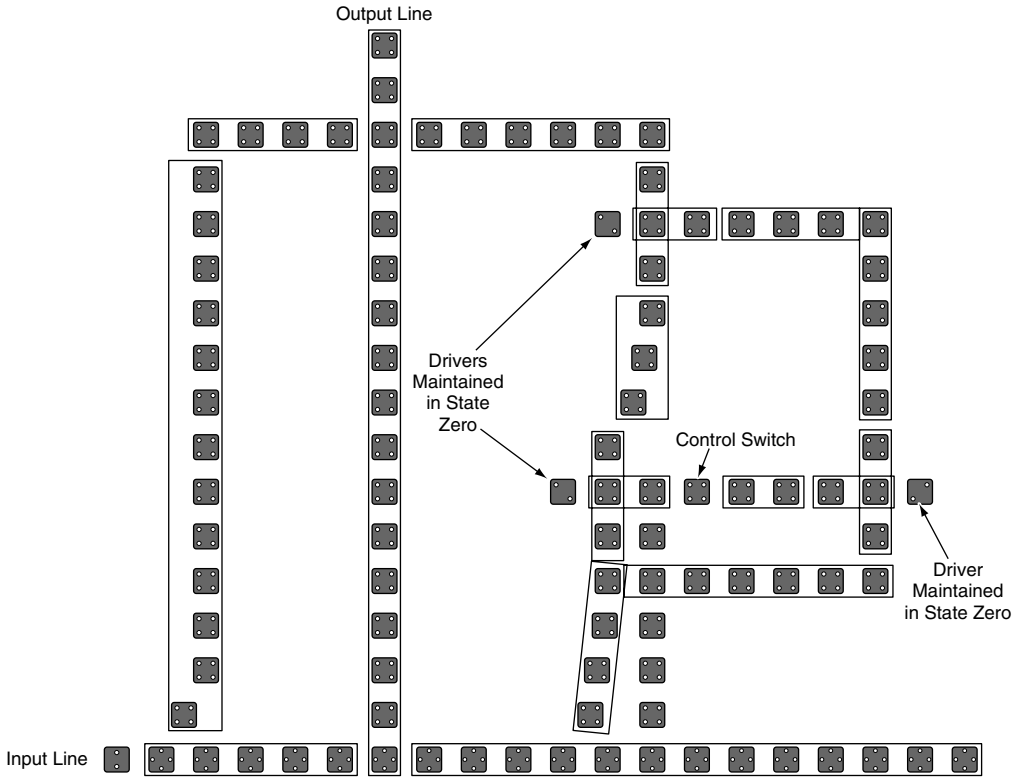


**DETAIL OF A CROSSPOINT SWITCH**

Figure 2. A **Crossbar Network** would be a coplanar assembly of QCA-based wires subdivided into QCA arrays excited by suitably timed clock signals.

lines cross a given output line, only one input line is allowed to put a signal on that output line; in other words, the connections between the other input lines and the given output line are required to be of high impedance in order to block signals.

Figure 2 depicts a proposed QCA-based crosspoint switch and a 3 × 3 crossbar network. The crosspoint switch would contain several branched QCA subarrays excited by suitably phased clock signals, and one of the quantum cellular automatons would serve as a control switch. The input signal $I_i$ would propagate toward the output line along one branch and, by suitable clocking and coupling, would be converted to another signal, $I_f$, propagating toward the output line along another branch. The application of a "0" signal to the control switch would cause $I_i$ and $I_f$ to be of the same state (both 0 or both 1), thereby causing the signal $I_i$ to be coupled onto the output line; in effect, the crosspoint switch would be in a low-impedance state. On the other hand, the application of a "1" signal to the control switch would cause $I_f$ to be the opposite of $I_i$, thereby preventing coupling of either $I_i$ or $I_f$ onto the output line; in effect, the crosspoint switch would be in a high-impedance state.

*This work was done by Amir Fijany, Nikzad Toomarian, Katayoon Modarress, and Matthew Spotnitz of Caltech for* **NASA's Jet Propulsion Laboratory**. *For further information, access the Technical Support Package (TSP)* ***free on-line at www.nasatech.com***.

*NPO-20855*

## Laterally Coupled Quantum-Dot Distributed-Feedback Lasers

These lasers show promise for single-frequency, single-spatial mode operation.

*NASA's Jet Propulsion Laboratory, Pasadena, California*

InAs quantum-dot lasers that feature distributed feedback and lateral evanescent-wave coupling have been demonstrated in operation at a wavelength of 1.3 μm. These lasers are prototypes of optical-communication oscillators that are required to be capable of stable single-frequency, single-spatial-mode operation.

A laser of this type (see figure) includes an active layer that comprises multiple stacks of InAs quantum dots embedded within InGaAs quantum wells. Distributed feedback is provided by gratings formed on both sides of a ridge by electron lithography and reactive-ion etching on the surfaces of an AlGaAs/GaAs waveguide. The lateral evanescent-wave coupling between the gratings and the wave propagating in the waveguide is strong enough to ensure operation at a single frequency, and the waveguide is thick enough to sustain a stable single spatial mode.

In tests, the lasers were found to emit continuous-wave radiation at temperatures up to about 90 °C. Side modes were found to be suppressed by more than 30 dB.

*This work was done by Yueming Qui, Pawan Gogna, Richard Muller, Paul Maker, and Daniel Wilson of Caltech and Andreas Stintz and Luke Lester of the University of New Mexico for* **NASA's Jet Propulsion Laboratory**. *For further information, access the Technical Support Package (TSP)* ***free on-line at www.nasatech.com***.

*In accordance with Public Law 96-517, the contractor has elected to retain title to this invention. Inquiries concerning rights for its commercial use should be addressed to*

*Intellectual Assets Office*
*JPL*
*Mail Stop 202-233*
*4800 Oak Grove Drive*
*Pasadena, CA 91109*
*(818) 354-2240*
*E-mail: ipgroup@jpl.nasa.gov*

*Refer to NPO-30503, volume and number of this* NASA Tech Briefs *issue, and the page number.*

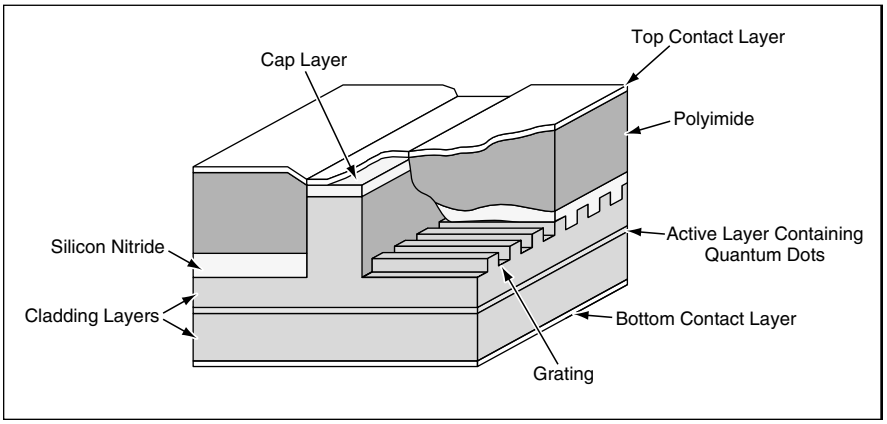


A **Laterally Coupled Quantum-Dot Distributed-Feedback Laser** contains structures that favor oscillation at a single frequency in a single spatial mode.

## Bit-Serial Adder Based on Quantum Dots

Adders like this could be used to develop advanced, compact computers.

*NASA's Jet Propulsion Laboratory, Pasadena, California*

A proposed integrated circuit based on quantum-dot cellular automata (QCA) would function as a bit-serial adder. This circuit would serve as a prototype building block for demonstrating the feasibility of quantum-dots computing and for the further development of increasingly complex and increasingly capable quantum-dots computing circuits. QCA-based bit-serial adders would be especially useful in that they would enable the development of highly parallel and systolic processors for implementing fast Fourier, cosine, Hartley, and wavelet transforms.

The proposed circuit would complement the QCA-based circuits described in "Implementing Permutation Matrices by Use of Quantum Dots" (NPO-20801), *NASA Tech Briefs*, Vol. 25, No. 10 (October 2001), page 42 and "Compact Interconnection Networks Based on Quantum Dots" (NPO-20855), which appears elsewhere in this issue. Those

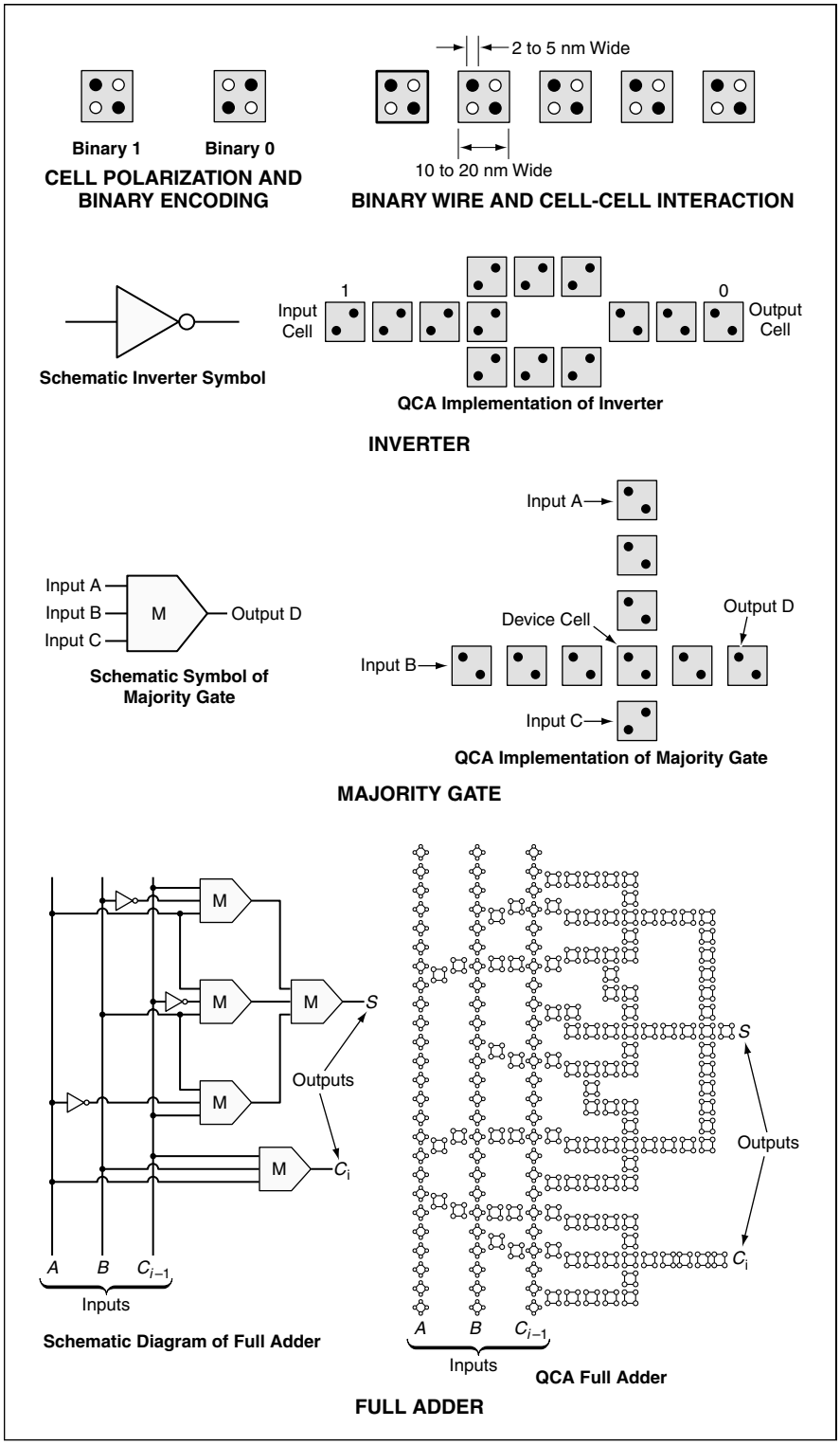


Figure 1. A **Full Adder** would be made of majority gates, inverters, and binary wires that would, in turn, be made of suitably arrayed quantum-dot cellular automata.

articles described the limitations of very-large-scale integrated (VLSI) circuitry and the major potential advantage afforded by QCA. To recapitulate: In a VLSI circuit, signal paths that are required not to interact with each other must not cross in the same plane. In contrast, for reasons too complex to describe in the limited space available for this article, suitably designed and operated QCA-based signal paths that are required not to interact with each other can nevertheless be allowed to cross each other in the same plane without adverse effect. In principle, this characteristic could be exploited to design compact, coplanar, simple (relative to VLSI) QCA-based networks to implement complex, advanced interconnection schemes.

To enable a meaningful description of the proposed bit-serial adder, it is necessary to further recapitulate the description of a quantum-dot cellular automation from the first-mentioned prior article: A quantum-dot cellular automaton contains four quantum dots positioned at the corners of a square cell. The cell contains two extra mobile electrons that can tunnel (in the quantum-mechanical sense) between neighboring dots within the cell. The Coulomb repulsion between the two electrons tends to make them occupy antipodal dots in the cell. For an isolated cell, there are two energetically equivalent arrangements (denoted polarization states) of the extra electrons. The cell polarization is used to encode binary information. Because the polarization of a nonisolated cell depends on Coulomb-repulsion interactions with neighboring cells, universal logic gates and binary wires could be constructed, in principle, by arraying QCA of suitable design in suitable patterns.

Again, for reasons too complex to describe here, in order to ensure accuracy and timeliness of the output of a QCA array, it is necessary to resort to an adiabatic switching scheme in which the QCA array is divided into subarrays, each controlled by a different phase of a multiphase clock signal. In this scheme, each subarray is given time to perform its computation, then its state is frozen by raising its interdot potential barriers and its output is fed as the input to the successor subarray. The successor subarray is kept in an unpolarized state so it does not influence the calculation of preceding subarray. Such a clocking scheme is consistent with pipeline computation in the sense that each different subarray can perform a different part of an overall computation. In other words, QCA arrays are inherently suitable for pipeline and, moreover, systolic computations. This sequential or pipeline aspect of QCA would be utilized in the proposed bit-serial adders.

The design of the proposed bit-serial adder incorporates a two-step innovation: (1) the design of an efficient QCA-based circuit that would function as a full adder, and (2) the design of QCA-based feedback loop with proper clocking that would enable the full adder to perform bit-serial addition. The full adder (see Figure 1) would contain three inverter gates and five majority gates. Given two

input bits (*A* and *B*) and one previous carry bit ($C_{i-1}$), this circuit would generate a sum bit (S) and a new carry bit ($C_i$).

A bit-serial adder would perform the addition operation on two sequences of input bits ($a_i$ and $b_i$ for $i$ = 1 to $n$) to generate a sequence of sum bits ($S_i$ for $i$ = 1 to $n$ + 1). To be able to perform the addition operation, the adder would have to be capable of storing the intermediate carry bits. A feedback loop could be used to effect such storage.

Figure 2 schematically depicts a bit-serial adder containing three majority gates and two inverter gates. This circuit could, optionally, be used as a full adder, in which role it would be more efficient, relative to the adder of Figure 1, in that it would contain fewer gates. The main advantage of the circuit of Figure 2 is that by use of suitable multiphase clocking, one could cause part of the circuit to act as a feedback loop for temporary storage of intermediate carry bits, thus enabling bit-serial addition. The ability of this circuit to perform bit-serial addition has been verified by computer simulation. However, several obstacles to practical implementation of a QCA-based bit-serial adder that could function without error at room temperature must still be overcome.

*This work was done by Amir Fijany, Nikzad Toomarian, Katayoon Modarress, and Matthew Spotnitz of Caltech for* **NASA's Jet Propulsion Laboratory**. *For further information, access the Technical Support Package (TSP)* ***free on-line at www.nasatech.com***.
*NPO-20869*

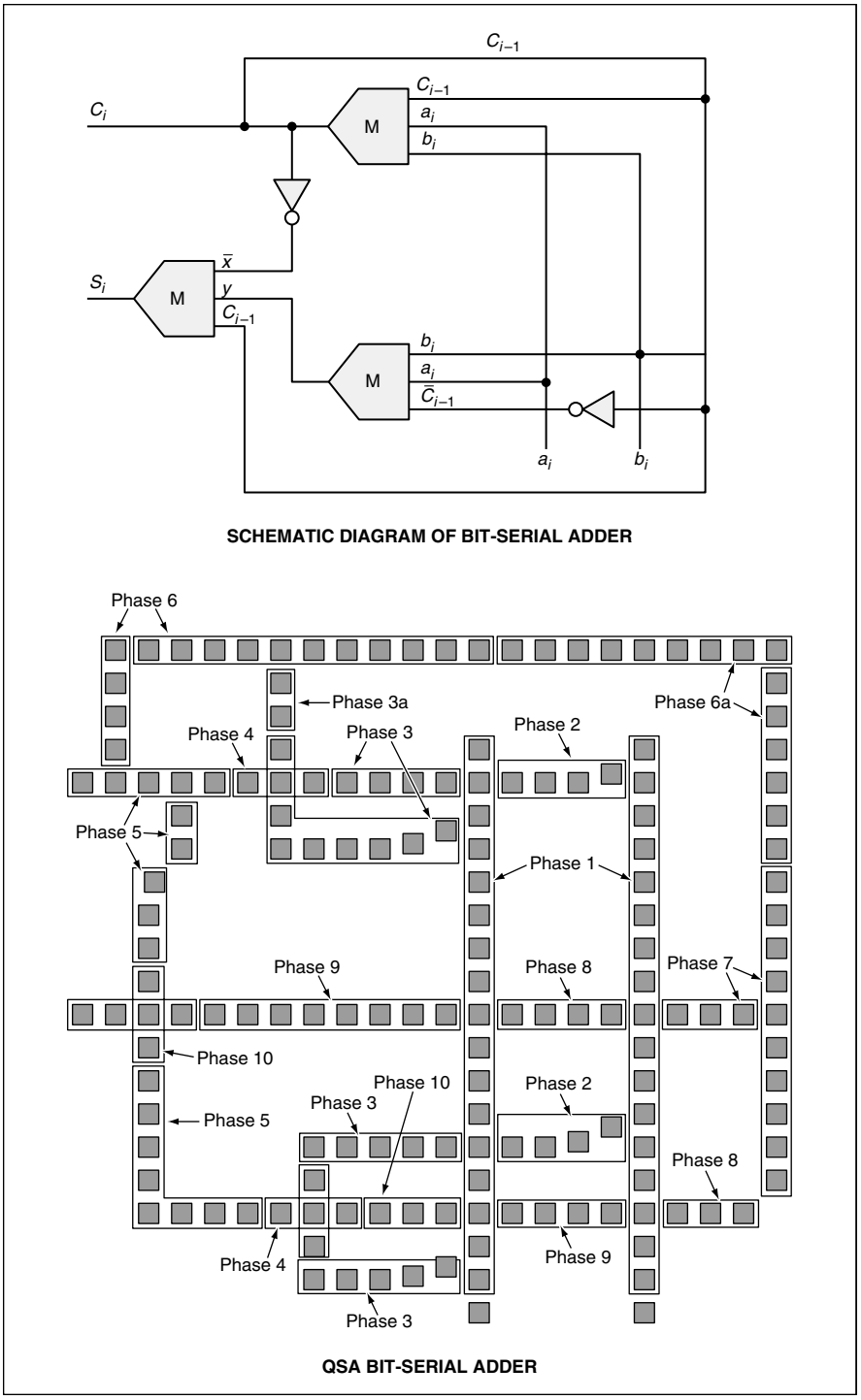


Figure 1. A **Full Adder** would be made of majority gates, inverters, and binary wires that would, in turn, be made of suitably arrayed quantum-dot cellular automata.

# Electronic Systems

## Hardware, Techniques, and Processes


15 Stabilized Fiber-Optic Distribution of Reference Frequency
15 Delay/Doppler-Mapping GPS-Reflection Remote-Sensing System
16 Ladar System Identifies Obstacles Partly Hidden by Grass


## Books and Reports


17 Survivable Failure Data Recorders for Spacecraft

## Stabilized Fiber-Optic Distribution of Reference Frequency

This system includes subsystems that provide short- and long-term stabilization.

*NASA's Jet Propulsion Laboratory, Pasadena, California*

An optoelectronic system distributes a reference signal of low noise and highly stabilized phase and frequency (100 MHz) from an atomic frequency standard to a remote facility at a distance up to tens of kilometers. The reference signal is transmitted to the remote station as amplitude modulation of an optical carrier signal propagating in an optical fiber. The stabilization scheme implemented in this system is intended particularly to suppress phase and frequency fluctuations caused by vibrations and by expansion and contraction of the optical fiber and other components in diurnal and seasonal heating and cooling cycles.

The system (see figure) comprises several subsystems, the main one being (1) a hydrogen-maser or linear-ion-trap frequency standard in an environmentally controlled room in a signal-processing center (SPC), (2) a stabilized fiber-optic distribution assembly (SFODA), (3) a compensated sapphire oscillator (CSO) in an environmentally controlled room in the remote facility, (4) thermally stabilized distribution amplifiers and cabling from the environmentally controlled room to end users, and (5) performance-measuring equipment. Two of these subsystems, considered as separate entities, were the subjects of prior *NASA Tech Briefs* articles: The SFODA was described in "Improved Stabilization of Delay in an Optical Fiber" (NPO-19353), Vol, 21, No. 2 (February 1997), page 4a; and "Alternative for Stabilization of Delay in an Optical Fiber" (NPO-19075), Vol. 21, No. 2 (February 1997), page 6a. The CSO was described in "Temperature-Compensated Sapphire Microwave Resonator" (NPO-19414), Vol. 20, No. 3 (March 1996), page 14a.

To recapitulate: The SFODA includes the transmitter in which the output of the frequency standard is used to modulate the optical distribution signal, the optical fiber used for long-distance transmission, a compensator reel (a wound, electrically controllable fiber-optic delay line in series with the long-distance optical fiber), signal retransmission optics in the remote facility, and equipment in the SPC that measures the overall round-trip propagation delay of the reference signal and adjusts the temperature of the compensator-reel to maintain the overall propagation delay as nearly constant as possible. The CSO is a sapphire-dielectric-ring microwave resonator that operates in a "whispering-gallery" electromagnetic mode and features a paramagnetic-spin-tuned design that provides temperature compensation for ultrahigh frequency stability.

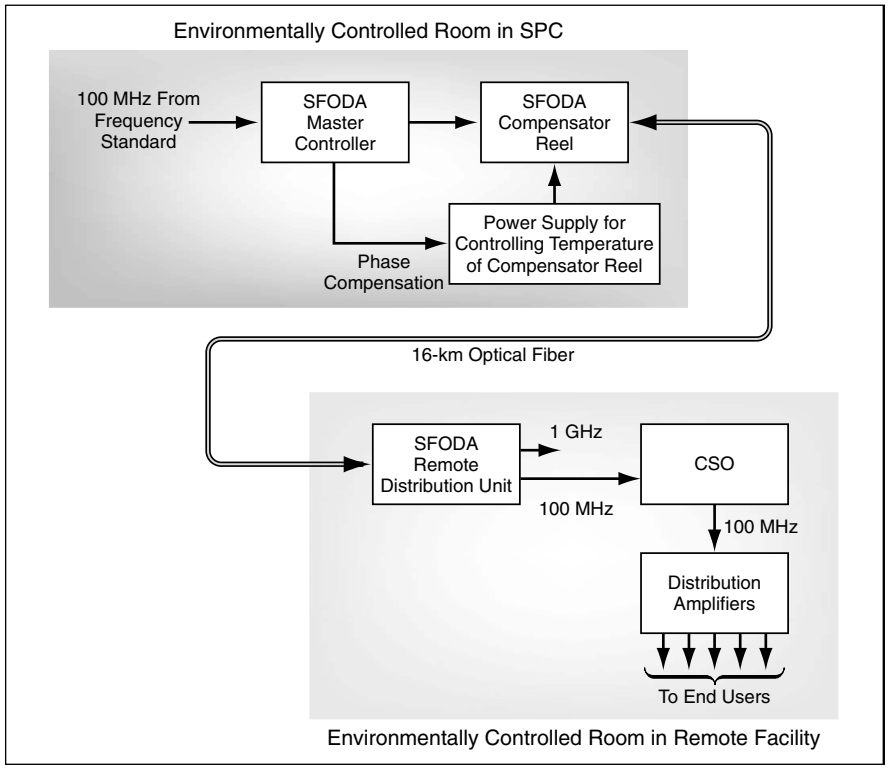


A **Frequency-Standard Signal** is transmitted over a long fiber-optic link augmented with equipment at both ends that stabilizes the output frequency and phase to a high degree.

The SFODA and the CSO work in unison in their environmentally controlled rooms to satisfy stringent requirements for stability of frequency and phase: While the SFODA helps to ensure long-term stability, the CSO helps to ensure short-term stability. In this system, the 100-MHz signal is first multiplied to 1 GHz before applying it as modulation to the optical carrier. At the remote site, a low-noise 100-MHz voltage-controlled oscillator (VCO) that is part of the SFODA is phase-locked to the 1-GHz signal to preserve coherence with the frequency standard. In turn, the CSO is phase-locked to the output of the VCO. The cleaned-up signal is then measured and distributed to end users.

*This work was done by Malcolm Calhoun, Robert Tjoelker, William Diener, G. John Dick, Rabi Wang, and Albert Kirk of Caltech for* **NASA's Jet Propulsion Laboratory**. *For further information, access the Technical Support Package (TSP)* ***free online at www.nasatech.com*** *NPO-30490*

## Delay/Doppler-Mapping GPS-Reflection Remote-Sensing System

This system offers capabilities beyond those of prior GPS-reflection remote-sensing systems.

*NASA's Jet Propulsion Laboratory, Pasadena, California*

A radio receiver system that features enhanced capabilities for remote sensing by use of reflected Global Positioning System (GPS) signals has been developed. This system was designed primarily for ocean altimetry, but can also be used for scatterometry and bistatic synthetic-aperture radar imaging. Moreover, it could readily be adapted to utilize navigation-satellite systems other than the GPS, including the Russian Global Navigation Satellite System

(GLONASS) and the proposed European Galileo system.

This remote-sensing system offers both advantages and disadvantages over traditional radar altimeters: One advantage of GPS-reflection systems is that they cost less because there is no need to transmit signals. Another advantage is that there are more simultaneous measurement opportunities — one for each GPS satellite in view. The primary disadvantage is that in comparison with radar signals, GPS signals are weaker, necessitating larger antennas and/or longer observations.

This GPS-reflection remote-sensing system was tested in aircraft and made to record and process both (1) signals coming directly from GPS satellites by means of an upward-looking antenna and (2) GPS signals reflected from the ground by means of a downward-looking antenna. In addition to performing conventional GPS processing, the system records raw signals for postprocessing as required.

The figure schematically depicts the airborne equipment part of the present system. Four synchronized GPS receiver front ends, each connected to a separate antenna, sample the complex (in-phase and quadrature) GPS L1 (1,575.42 MHz) and L2 (1,227.6) signals at a rate of 20.456 MHz. The sampling clock in one receiver front end is used as a master clock for synchronizing all four receivers and two digital data recorders. The raw samples are fed through the digital data recorders for storage on two 300-GB arrays of hard disks. Subsequently, the digitized samples are processed by software that performs functions similar to those of GPS hardware receivers, plus additional processing of the reflected signals.

Whereas prior such systems have utilized the delay information in the GPS signals, this system also utilizes the Doppler shifts of the signals to increase precision and extract additional information about the terrain or water surface under observation. The system offers 160 to 320 times the data-collection bandwidth of prior GPS-reflection remote-sensing systems. Moreover, unlike other such systems that do not have reprocessing capability, this system affords much greater flexibility because it can be made to reprocess the recorded signal data at will.

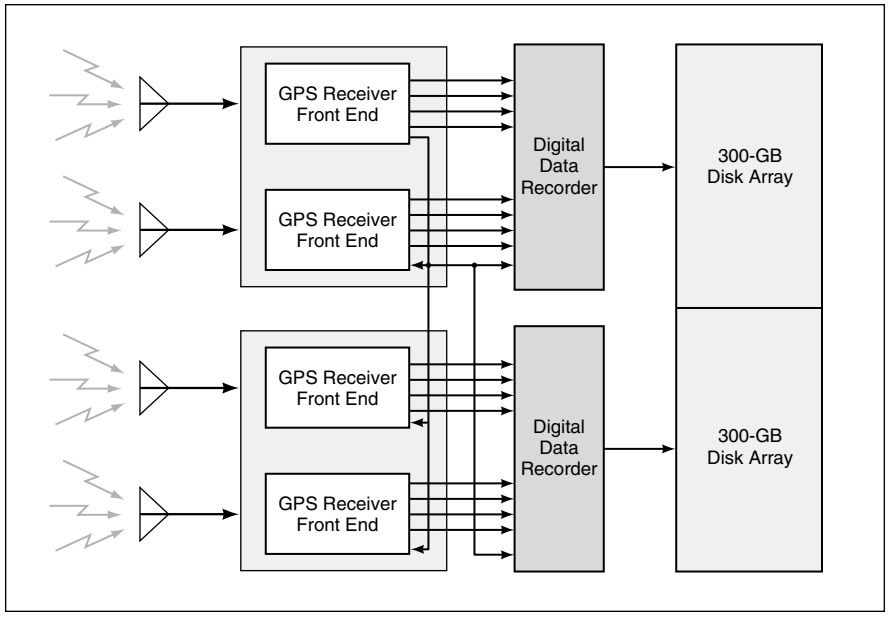


This **Airborne Subsystem** samples direct and reflected GPS signals and records the resulting data. Later, the data are uploaded to general-purpose computers for processing by software that performs a variety of standard and custom GPS receiver functions.

The software signal-processing functions in this system include detection of signals; tracking of phases and delays; mapping of delay, Doppler, and delay/Doppler waveforms; dual-frequency (L1 and L2) processing; coherent integrations as short as 125 μs; decoding of navigation messages; and precise time tagging of observable quantities. The software can perform these functions on all detectable satellite signals without dead time. Custom signal-processing features can easily be included: For example, in principle, data collected over the ocean by this system can be processed to extract mean sea height, wind speed and direction, and significant wave height; data collected over land can be processed to extract measures of soil moisture and biomass; and data collected over ice can be processed to obtain estimates of the ice age, thickness, and surface density.

*This work was done by Stephen Lowe, Peter Kroger, Garth Franklin, John LaBrecque, Jesse Lerma, Michael Lough, Martin Marcin, Ronald Muellerschoen, Donovan Spitzmesser, and Lawrence Young of Caltech for* **NASA's Jet Propulsion Laboratory**. *For further information, access the Technical Support Package (TSP)* ***free on-line at www.nasatech.com***.
*NPO-30385*

## Ladar System Identifies Obstacles Partly Hidden by Grass

A robot moving cross country (e.g., an agricultural robot) could avoid obstacles.

*NASA's Jet Propulsion Laboratory, Pasadena, California*

A ladar-based system now undergoing development is intended to enable an autonomous mobile robot in an outdoor environment to avoid moving toward trees, large rocks, and other obstacles that are partly hidden by tall grass. The design of the system incorporates the assumption that the robot is capable of moving through grass and provides for discrimination between grass and obstacles on the basis of geometric properties extracted from ladar readings as described below.

The system (see figure) includes a ladar system that projects a range-measuring pulsed laser beam that has a small angular width of $\Delta$ radians and is capable of measuring distances of reflective objects from a minimum of $d_{min}$ to a maximum of $d_{max}$. The system is equipped with a rotating mirror that

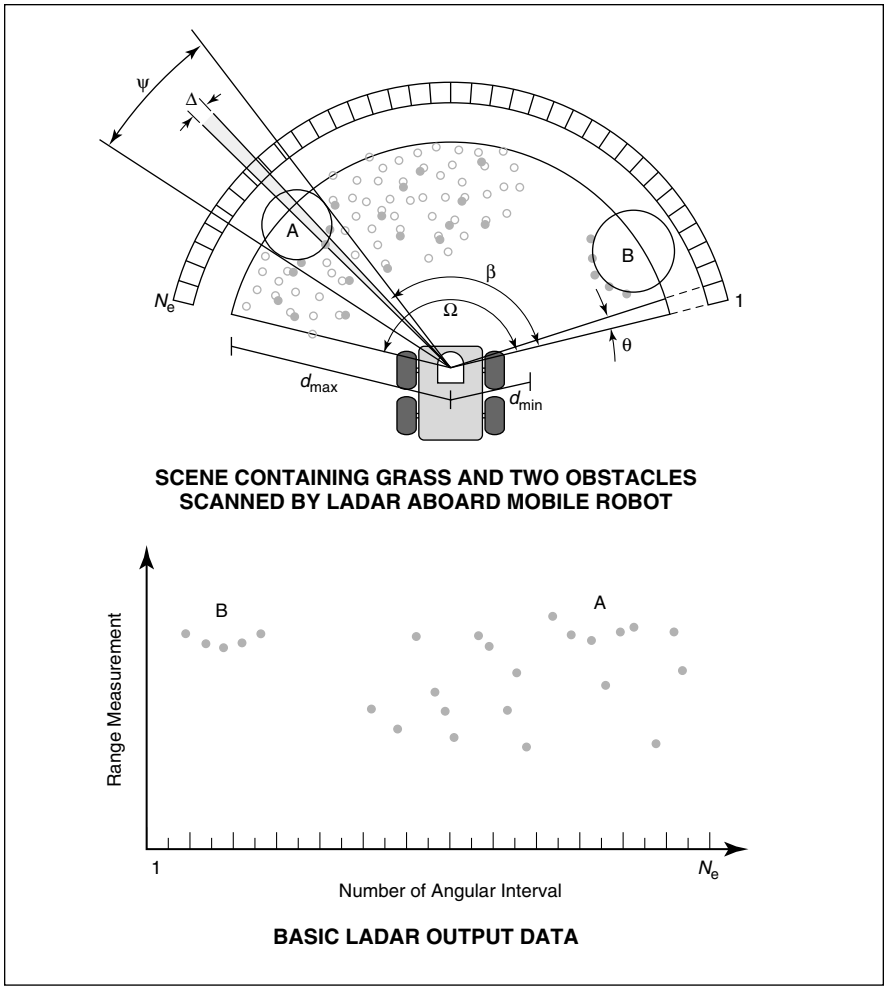


**Ladar Aboard a Robotic Vehicle** scans through a fan-shaped area to measure distances to nearby objects, which are represented here by circles. The small circles represent stalks of grass. Large circle A represents a tree trunk partly hidden by grass; large circle B represents a tree trunk in the clear.

scans the beam through a relatively wide angular range of $\Omega$ in a horizontal plane at a suitable small height above the ground. Successive scans are performed at time intervals of $\tau$ seconds. During each scan, the laser beam is fired at relatively small angular intervals of $\theta$ radians to make range measurements, so that the total number of range measurements acquired in a scan is $N_e = \Omega/\theta$.

The basic ladar output data for each scan consist of a range measurement for each of the $N_e$ angular intervals. These data are processed by an algorithm that classifies objects as either foliage (that is, grass stalks) or not foliage (that is, obstacles). Objects to which the algorithm cannot assign the classification "foliage" with a sufficiently high degree of confidence are conservatively classified as "not foliage" to ensure avoidance of obstacles.

The classification is made on the basis of three locality principles that are here described by reference to object A at scan angle $\beta$ in the figure. The first principle is one of locality in both space and time: If A is an obstacle and is found at angle $\beta$ at time $t$, then it will be found at an angle near $\beta$ at time $t + \tau$. The second principle is that if A is an obstacle, it must subtend a substantial angle $\psi$ and all laser-beam directions that intersect A must lie within the angular range $\beta \pm \psi$. The third principle is one of spatial locality of the gaps between grass stalks that enable the laser beam to penetrate the foliage and reach object A: If the laser beam penetrates the foliage and hits A when aimed at angle $\beta$, then it is also likely to do so when aimed at angle $\beta \pm \Delta$. These locality principles hold for any combination of motions of the robot and the obstacles, as long as the angular sampling interval ($\theta$) and the time between consecutive scans ($\tau$) are sufficiently small.

*This work was done by Andres Castano of Caltech for* **NASA's Jet Propulsion Laboratory**. *For further information, access the Technical Support Package (TSP)* ***free on-line at www.nasatech.com***.
*NPO-30597*

# Books and Reports

## Survivable Failure Data Recorders for Spacecraft

A spacecraft may be unable to communicate critical data associated with a serious or catastrophic failure. A brief report proposes a system, somewhat like a commercial aircraft "black box," for retrieving these data. A microspacecraft attached to the prime spacecraft would continually store recent critical data from that spacecraft. If either spacecraft detected certain serious conditions of the prime spacecraft, the microspacecraft would separate from the prime spacecraft and independently transmit the stored data to Earth. Supplemental data, acquired from sensors onboard the microspacecraft, could be added to this transmission. For example, the orientation and angular rates of the prime spacecraft immediately before separation as well as pictures taken of the prime spacecraft after separation could be included. Functional enhancements over aircraft black boxes include the separation from the prime vehicle (which gains independence from the fate of that vehicle), wireless transmission of data (making physical black box recovery unnecessary), and the optional acquisition of supplemental sensor data.

*This work was carried out by John Carraway and David Collins of Caltech for* **NASA's Jet Propulsion Laboratory**. *To obtain a copy of the report "Spacecraft 'Black Box' Flight Recorder," access the Technical Support Package (TSP)* ***free on-line at www.nasatech.com***. *NPO-20842*

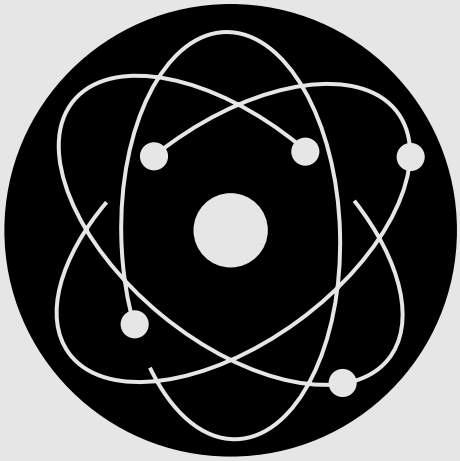

# Physical Sciences

## Hardware, Techniques, and Processes


21 Fiber-Optic Ammonia Sensors
21 Silicon Membrane Mirrors With Electrostatic Shape Actuators
22 Nanoscale Hot-Wire Probes for Boundary-Layer Flows
22 Theodolite With CCD Camera for Safe Measurement of Laser-Beam Pointing
23 Efficient Coupling of Lasers to Telescopes With Obscuration
24 Aligning Three Off-Axis Mirrors With Help of a DOE
25 Calibrating Laser Gas Measurements by Use of Natural $CO_2$
26 Laser Ranging Simulation Program
27 Micro-Ball-Lens Optical Switch Driven by SMA Actuator


## Books and Reports


28 Evaluation of Charge Storage and Decay in Spacecraft Insulators

## Fiber-Optic Ammonia Sensors

Reversible, colorimetric fiber-optic sensors are undergoing development for use in measuring concentrations of ammonia in air at levels relevant to human health [0 to 50 parts per million (ppm)]. A sensor of this type includes an optical fiber that has been modified by replacing a portion of its cladding with a polymer coat that contains a dye that reacts reversibly with ammonia and changes color when it does so. The change in color is measured as a change in the amount of light transmitted from one end of the fiber to the other. Responses are reversible and proportional to the concentration of ammonia over the range from 9 to 175 ppm and in some cases the range of reversibility extends up to 270 ppm. The characteristic time for the response of a sensor to rise from 10 to 90 percent of full scale is about 25 seconds. These sensors are fully operational in pure carbon dioxide and are not adversely affected by humidity.

*This work was done by Michael T. Carter of Eltron Research, Inc., for* **Kennedy Space Center**. *For further information, please contact:*

*Dr. Michael Carter*
*4600 Nautilus Court South*
*Boulder, CO 80301-3241*
*Tel. No.: (303) 530-0263 Ext. 113*
*E-mail: mtcarter@eltronresearch.com*

*KSC-12130*

## Silicon Membrane Mirrors With Electrostatic Shape Actuators

Precise shapes could be maintained over a wide temperature range.

*NASA's Jet Propulsion Laboratory, Pasadena, California*

Efforts are under way to develop deformable mirrors equipped with microscopic electrostatic actuators that would be used to maintain their reflective surfaces in precise shapes required for their intended applications. Unlike actuators that depend on properties of materials (e.g., piezoelectric and electrostrictive actuators), electrostatic actuators are effective over a wide temperature range. A mirror of the present type would be denoted a MEMS-DM (for microelectromechanical system deformable mirror). The reflective surface of such a mirror would be formed on a single-crystal silicon membrane that would be attached by posts to a silicon actuator membrane that would, in turn, be attached by posts to a rigid silicon base (see figure).

The actuator membrane would serve as the upper electrode of a capacitor. Multiple lower electrodes, each occupying a conveniently small fraction of the total area, would be formed on an electrically insulating oxide layer on the base, thereby defining a multiplicity of actuator pixels. The actuator membrane would be corrugated in a pattern that would impart mechanical compliance needed for relaxation of operational and fabrication-induced stresses and to minimize the degree of nonlinearity of deformations. The compliance afforded by the corrugations would also help to minimize the undesired coupling of deformations between adjacent pixels (a practical goal being to keep the influence coefficient between adjacent pixels below 10 percent).

The mirror and actuator membranes and posts would be fabricated partly by surface and partly by bulk micromachining of silicon. Other micromachining techniques that are in common use in the integrated-circuit industry could be used to integrate driver and control electronic circuits into the actuator structure. The base, actuator, and mirror layers would be assembled by use of the process described in "Wafer-Level Membrane-Transfer Process for Fabricating MEMS" (NPO-21088), *NASA Tech Briefs*, Vol. 27, No. 1 (January 2003), page 58.

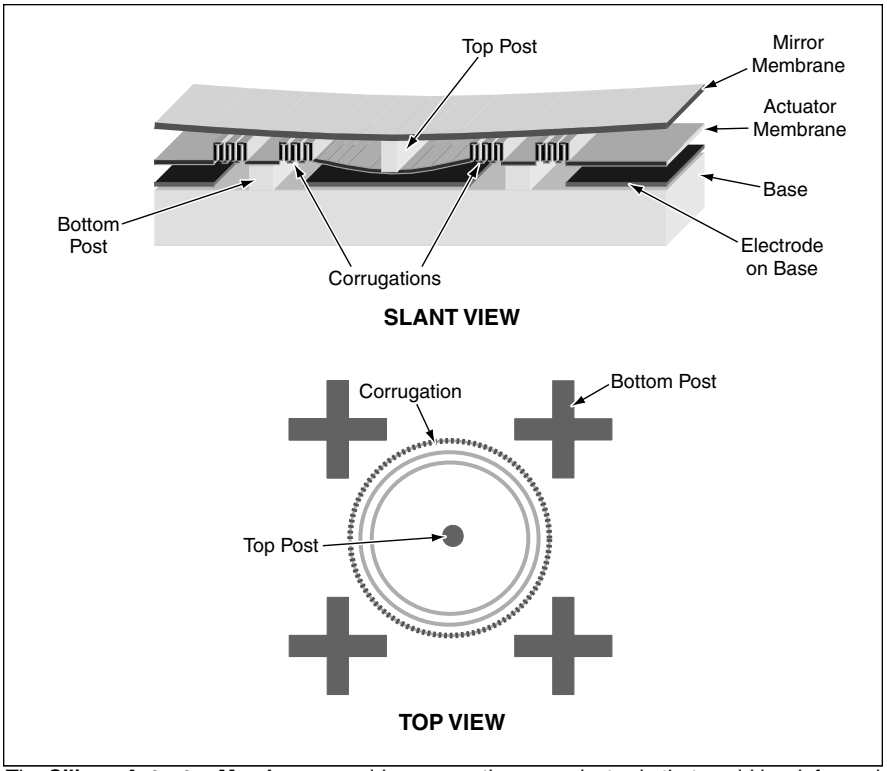


The **Silicon Actuator Membrane** would serve partly as an electrode that could be deformed by electrostatic attraction to the electrodes on the base. The deformation would be transferred to the mirror membrane.

The center-to-center distance of adjacent pixels could be as small as about 100 μm. A typical design would call for a center-to-center distance of 200 μm and a maximum deflection of about 2 μm. Calculations for a representative example of such a design, in which the actuator in one pixel generated a force of $10^{-4}$ N, yielded an estimated actuator-membrane deflection of 0.03 μm and mirror-membrane deflection of 0.4 μm. The adjacent-pixel influence coefficient in this example was found to be less than 10 percent.

*This work was done by Eui-Hyeok Yang of* **NASA's Jet Propulsion Laboratory**. *For further information, access the Technical Support Package (TSP)* ***free on-line at www.nasatech.com***.

*NPO-21120*

# Nanoscale Hot-Wire Probes for Boundary-Layer Flows

Flow parameters near walls would be measured with unprecedented resolution.

*Langley Research Center, Hampton, Virginia*

Hot-wire probes having dimensions of the order of nanometers have been proposed for measuring temperatures (and possibly velocities) in boundary-layer flows at spatial resolutions much finer and distances from walls much smaller than have been possible heretofore. The achievable resolutions and minimum distances are expected to be of the order of tens of nanometers — much less than a typical mean free path of a molecule and much less than the thickness of a typical flow boundary layer in air at standard temperature and pressure. An additional benefit of the small scale of these probes is that they would perturb the measured flows less than do larger probes.

The hot-wire components of the probes would likely be made from semiconducting carbon nanotubes or ropes of such nanotubes. According to one design concept, a probe would comprise a single nanotube or rope of nanotubes laid out on the surface of an insulating substrate between two metallic wires. According to another design concept, a nanotube or rope of nanotubes would be electrically connected and held a short distance away from the substrate surface by stringing it between two metal electrodes. According to a third concept, a semiconducting nanotube or rope of nanotubes would be strung between the tips of two protruding electrodes made of fully conducting nanotubes or ropes of nanotubes. The figure depicts an array of such probes that could be used to gather data at several distances from a wall.

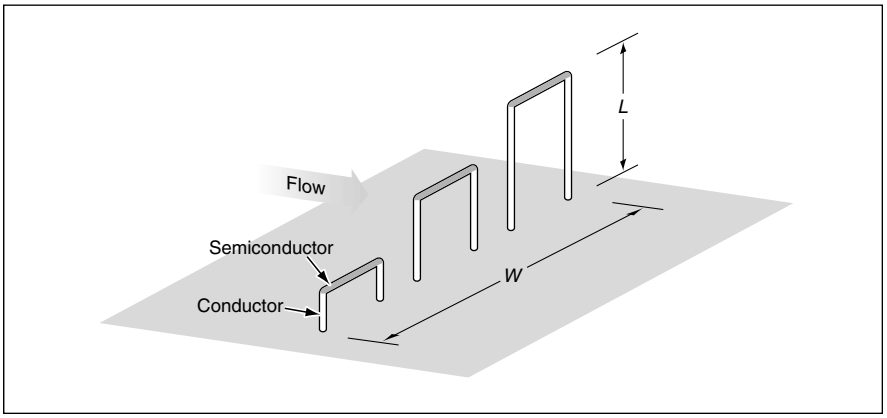


**Nanoscale Hot-Wire Probes** would be used to characterize a flow at several distances from a surface, typically ranging from tens of nanometers to a few micrometers. The lateral dimension, *W*, of the array of probes would be made much less than the expected characteristic dimension of lateral nonuniformity of the flow. The distance from the surface (*L*) of the most distant probe would be made much less than the expected thickness of the boundary layer of the flow.

It will be necessary to develop techniques for fabricating the probes. It will also be necessary to determine whether the probes will be strong enough to withstand the aerodynamic forces and impacts of micron-sized particles entrained in typical flows of interest.

The proposed probes may or may not be based on the same principles as those of larger hot-wire anemometer and thermometer probes. The potential for unexpected effects (e.g., quantized current or heat flow) in the nanometer size range makes it necessary to perform research on the basic physics of these probes in order to be able to calibrate them, operate them under conditions (e.g., constant current, or constant temperature) that will yield useful data, and interpret their thermal and electrical responses in terms of flow parameters.

*This work was done by Ken T. Tedjojuwono and Gregory C. Herring of* **Langley Research Center**. *For further information, access the Technical Support Package (TSP)* ***free on-line at www.nasatech.com***.

*LAR-16223*

# Theodolite With CCD Camera for Safe Measurement of Laser-Beam Pointing

The risk of looking directly at the laser beam is eliminated.

*Goddard Space Flight Center, Greenbelt, Maryland*

The simple addition of a charge-coupled-device (CCD) camera to a theodolite makes it safe to measure the pointing direction of a laser beam. The present state of the art requires this to be a custom addition because theodolites are manufactured without CCD cameras as standard or even optional equipment.

A theodolite is an alignment telescope equipped with mechanisms to measure the azimuth and elevation angles to the sub-arcsecond level. When measuring the angular pointing direction of a Class II laser with a theodolite, one could place a calculated amount of neutral density (ND) filters in front of the theodolite's telescope. One could then safely view and measure the laser's boresight looking through the theodolite's telescope without great risk to one's eyes. This method for a Class II visible wavelength laser is not acceptable to even consider tempting for a Class IV laser and not applicable for an infrared (IR) laser. If one chooses insufficient attenuation or forgets to use the filters, then looking at the laser beam through the theodolite could cause instant blindness.

The CCD camera is already commercially available. It is a small, inexpensive, black-and-white CCD circuit-board-level camera. An interface adaptor was designed and fabricated to mount the camera onto the eyepiece of the specific theodolite's viewing telescope.

Other equipment needed for operation of the camera are power supplies, cables, and a black-and-white television monitor. The picture displayed on the monitor is equivalent to what one would see when looking directly through the theodolite. Again, the additional advantage afforded by a cheap black-and-white CCD camera is that it is sensitive to infrared as well as to visible light. Hence, one can use the camera coupled to a theodolite to measure the pointing of an infrared as well as a visible laser.

Just as it is necessary to use filters to protect the eye when looking directly through the theodolite, it is necessary to use filters to protect the CCD camera and the theodolite's internal optics against damage by the laser beam. One should be aware of the metrology accuracy requirements and use high-quality filters for tighter accuracy metrology requirements. The main benefits of using the CCD camera are being able to view the IR laser and for high-powered lasers, that in the event that one chooses insufficient attenuation or forgets to use the filters, the equipment may be damaged, but there is no injury to the human eye.

*This work was done by Julie A. Crooke of* **Goddard Space Flight Center**. *For further information, access the Technical Support Package (TSP)* ***free on-line at www.nasatech.com***.
*GSC-14469*

## Efficient Coupling of Lasers to Telescopes With Obscuration

Two proposed techniques offer advantages over two prior techniques.

*NASA's Jet Propulsion Laboratory, Pasadena, California*

Two techniques have been proposed to increase the efficiency of coupling of light from lasers to Cassegrain telescopes and, in general, telescopes with secondary or tertiary mirror obscuration. The need to increase the efficiency of coupling arises in laser transmitters of lidar and free-space optical communication systems that utilize Cassegrain telescopes. The vignetting caused by the secondary reflector and baffle in such a telescope reduces the transmitted power by a large fraction because (1) the obscured area is central and is a significant fraction of the telescope aperture and (2) the cross-sectional intensity profile of a typical laser beam is Gaussian, so that intensity is greatest in the obscured central area.

In a technique proposed previously for increasing the efficiency of coupling, an optical assembly comprising an axicon device and a folding mirror that would render the solid laser beam annular — in effect, turning the laser beam inside out — so that the laser light would be concentrated into an annular cross section that would not be obscured by the secondary reflector and baffle. Hence, most or all of the light would be coupled into the output beam.

Another prior efficiency-enhancing technique is denoted subaperture illumination. In this technique, the laser beam is displaced laterally with respect to the optical axis of the secondary reflector, such that the beam impinges on an off-axis subaperture of the primary reflector that is not obscured by the secondary reflector and baffle.

The disadvantages of the axicon approach are that it is difficult to fabricate an axicon device and that a small misalignment can strongly degrade its functionality. The disadvantage of the subaperture-illumination approach is that the beam transmitted by the telescope diverges more than it would if the entire aperture were illuminated.

In the first of the techniques now proposed, one would use a folding mirror in combination with a prism beam slicer that would function partly similarly to an axicon. Like an axicon device, the prism slicer would be an afocal refractive and reflective optical element. Like an axicon, the prism beam slicer would utilize both transmitting and reflecting optical surfaces. In the meridional cross-sectional detail in Figure 1, the prism slicer would look exactly like the axicon device.

Unlike the axicon device, the prism beam slicer would not have any curved optical surfaces: this would make it easier to fabricate and would make its functionality less sensitive to misalignment. The prism beam slicer

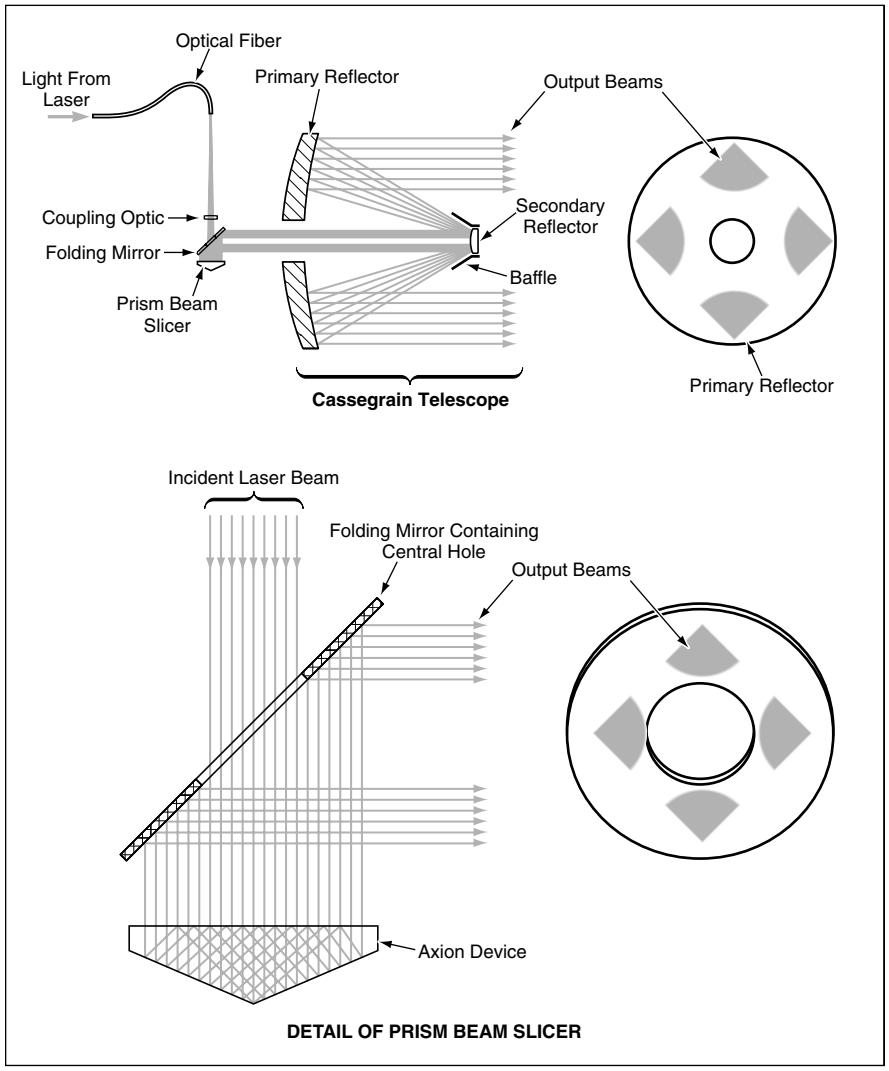


Figure 1. The **Prism Beam Slicer and Folding Mirror** in a laser transmitter would concentrate most of the laser light into off-axis sector-of-circle cross sections that would not be obscured by the secondary reflector and baffle.

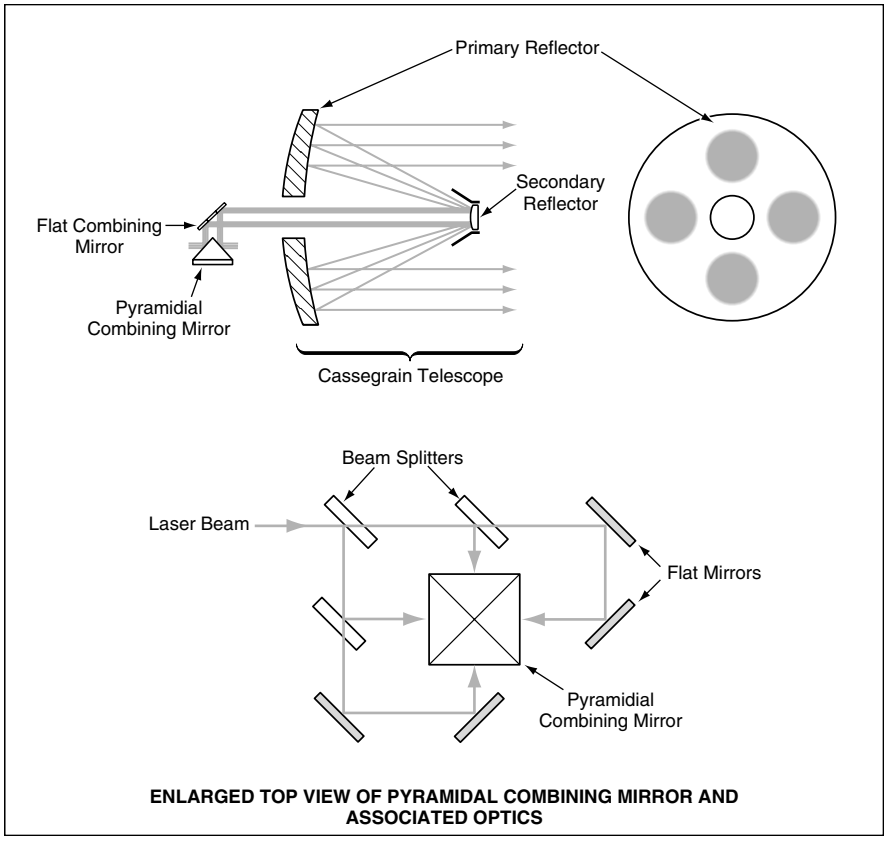


Figure 2. The **Laser Beam Would Be Split** in four and then recombined in such a manner as to illuminate the primary mirror in four unobscured subapertures.

would slice the laser beam into two or more beams that would have sector-of-circle cross sections, and that would be arranged symmetrically about the optical axis in unobscured off-axis positions. The difference between the axicon device and the prism beam slicer is that instead of a conical rear surface, the prism beam slicer would have an even number of flat rear surfaces in a pyramidal configuration at the same angle as that of the conical surface in the axicon device. If the number of pyramidal surfaces were made infinite, the prism beam splitter would revert to the axicon device.

The second technique now proposed would be a combination of the subaperture-illumination technique with a beam-splitting/beam-combining technique. As shown in Figure 2, the laser beam would be split into four beams that would be made to impinge on four faces of a pyramidal combining mirror and then further reflected by a flat combining mirror to generate four beams that would be parallel to the optical axis and would strike the primary mirror at unobscured off-axis positions 90° apart.

*This work was done by Hamid Hemmati and Norman Page of Caltech for* **NASA's Jet Propulsion Laboratory**. *For further information, access the Technical Support Package (TSP)* ***free on-line at www.nasatech.com***.

*In accordance with Public Law 96-517, the contractor has elected to retain title to this invention. Inquiries concerning rights for its commercial use should be addressed to*

*Intellectual Assets Office*
*JPL*
*Mail Stop 202-233*
*4800 Oak Grove Drive*
*Pasadena, CA 91109*
*(818) 354-2240*
*E-mail: ipgroup@jpl.nasa.gov*

*Refer to NPO-30574, volume and number of this* NASA Tech Briefs *issue, and the page number.*

# Aligning Three Off-Axis Mirrors With Help of a DOE

Precise lithographic fabrication would solve a large part of the alignment problem.

*NASA's Jet Propulsion Laboratory, Pasadena, California*

A proposed method based on the use of a special-purpose diffractive optical element (DOE) would simplify (relative to prior methods) the alignment of three off-axis mirrors that constitute an imaging optical system. The method would exploit the fact that a DOE can be fabricated lithographically with high accuracy by electron-beam lithography in a thin film of poly(methyl methacrylate). The method would effectively transfer much of the problem of obtaining the needed accuracy from the mechanical-mirror-alignment domain to the lithographic domain. Unlike other methods that depend on specific symmetries (e.g., sphericity and/or concentricity), this method is expected to apply with equal ease and accuracy to mirrors of any configuration — including aspherical, decentered mirrors.

Assuming that one of the mirrors of a general three-mirror imaging optical system can serve as a reference for the alignment of the other two mirrors, such a system has 12 degrees of freedom in alignment. In the proposed method, one would use an interferometer in combination with a DOE to effect precise and relatively rapid and easy alignment of two of the mirrors with respect to each other, thus reducing the alignment task to that of the six degrees of freedom of the remaining mirror.

The figure depicts a representative three-mirror off-axis imaging system, wherein the primary and tertiary mirrors (M1 and M3, respectively) are concave and the secondary mirror (M2) is convex. The DOE for aligning this system would be fabricated on the right surface of an optical flat and could be made to have either negative or positive focusing power, depending on the requirements of the specific application. The DOE could be designed to be placed at any convenient distance from M1 and M3 — again, depending on the application.

The DOE would be illuminated with light coming from the left, generated by an interferometer. First, assuming the optical flat is of high quality, the plane of the DOE would be aligned perpendicular to the collimated beam by use of light reflected from the left face of the optical flat. The DOE would comprise two independent areas: one dedicated to M1, the other to M3. The portions of the collimated beam passing through those areas would be diffracted towards the corresponding mirrors. A mask, not shown in the figure, could be used to prevent light from

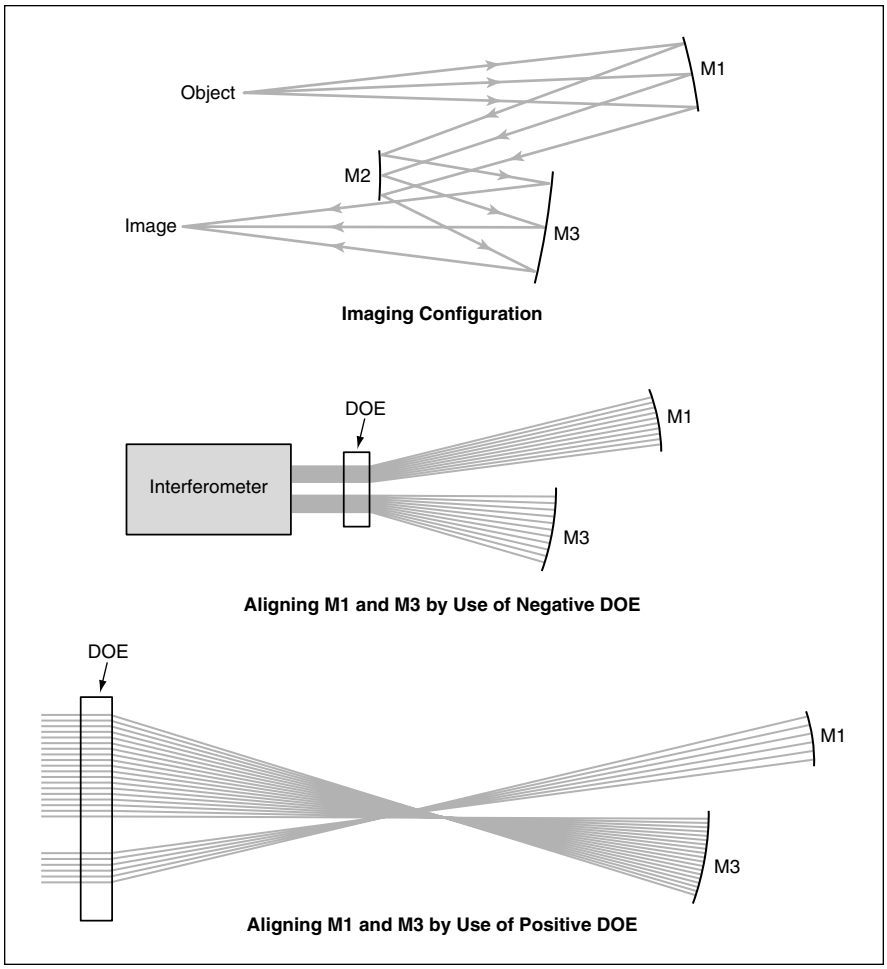


**Three Mirrors Would Be Aligned** with a DOE and, hence, with each other, in a sequence of interferometric procedures that would involve no more than six degrees of freedom of adjustment at one time.

passing through the rest of the area of the optical flat. Light rays reflected from M1 and M3 would retrace their paths through the DOE and would propagate leftward to the interferometer.

One would adjust the position and orientation of each of M1 and M3 in an effort to minimize the number of fringes in its portion of the interferogram. Such adjustments are commonplace in interferometry and can be performed easily. Once these adjustments were complete, M1 and M3 would be in alignment with the DOE and, hence, with each other.

With M1 and M3 thus fixed, one could align M2 by performing similar adjustments on M2 while observing the interferogram of the entire optical system in double pass, as is standard practice. For this purpose, it is necessary to generate an object beam with sufficient accuracy. For an infinitely distant object, it would suffice to remove the DOE and rotate the assembly of M1, M2, and M3 by a prescribed amount that can be easily calculated. The collimated beam from the interferometer would then act as object beam. For an object at a finite distance, one would place a focusing lens in front of the interferometer to generate a spherical wavefront, which could then be made to pass through a pinhole that could be fabricated at an otherwise unoccupied area of the DOE. The position of the pinhole could be known with high accuracy, inasmuch as it would be controlled during fabrication of the DOE.

By virtue of the precisely known geometric relationships between (1) the position of the pinhole and the rest of the DOE and (2) the DOE and the mirrors, the geometric relationship between the position of the pinhole and the object would thus also be known. The whole assembly could then be translated to the required coordinates, making it possible to use the interferometer beam as the object beam for final testing and alignment.

*This work was done by Pantazis Mouroulis and Daniel Wilson of Caltech for* **NASA's Jet Propulsion Laboratory**. *For further information, access the Technical Support Package (TSP)* ***free on-line at www.nasatech.com***.
*NPO-30279*

# Calibrating Laser Gas Measurements by Use of Natural $CO_2$

Every spectral scan includes a calibration line.

*NASA's Jet Propulsion Laboratory, Pasadena, California*

An improved method of calibration has been devised for instruments that utilize tunable lasers to measure the absorption spectra of atmospheric gases in order to determine the relative abundances of the gases. In this method, $CO_2$ in the atmosphere is used as a natural calibration standard. Unlike in one prior calibration method, it is not necessary to perform calibration measurements in advance of use of the instrument and to risk deterioration of accuracy with time during use. Unlike in another prior calibration method, it is not necessary to include a calibration gas standard (and the attendant additional hardware) in the instrument and to interrupt the acquisition of atmospheric data to perform calibration measurements.

In the operation of an instrument of this type, the beam from a tunable diode laser or a tunable quantum-cascade laser is directed along a path through the atmosphere, the laser is made to scan in wavelength over an infrared spectral region that contains one or two absorption spectral lines of a gas of interest, and the transmission (and, thereby, the absorption) of the beam is measured. The concentration of the gas of interest can then be calculated from the observed depth of the absorption line(s), given the temperature, pressure, and path length.

$CO_2$ is nearly ideal as a natural calibration gas for the following reasons: $CO_2$ has numerous rotation/vibration infrared spectral lines, many of which are near absorption lines of other gases. The concentration of $CO_2$ relative to the concentrations of the major constituents of the atmosphere is well

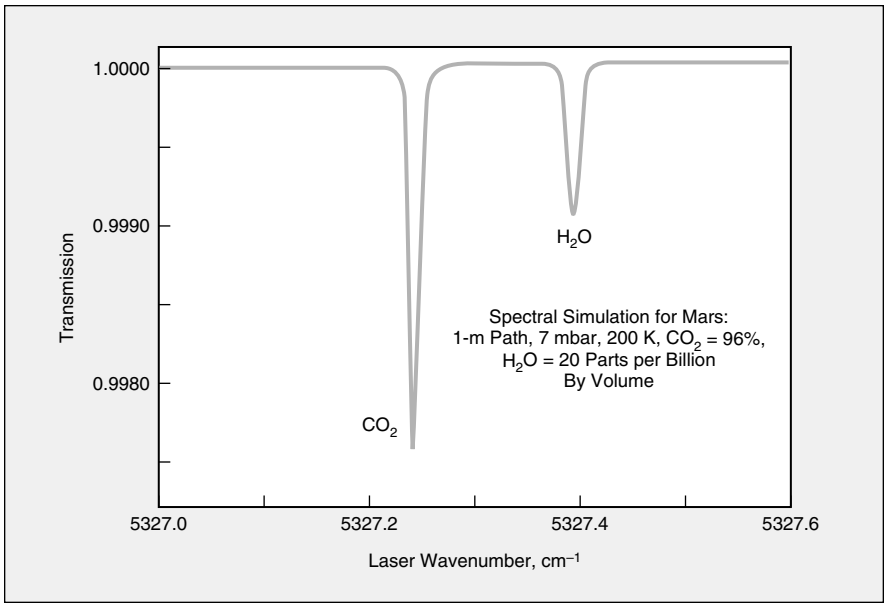


Figure 1. These **Simulated Spectral Transmission Measurements** illustrate the present method as applied to a wave-number range that contains absorption lines of $N_2O$ and $CO_2$.

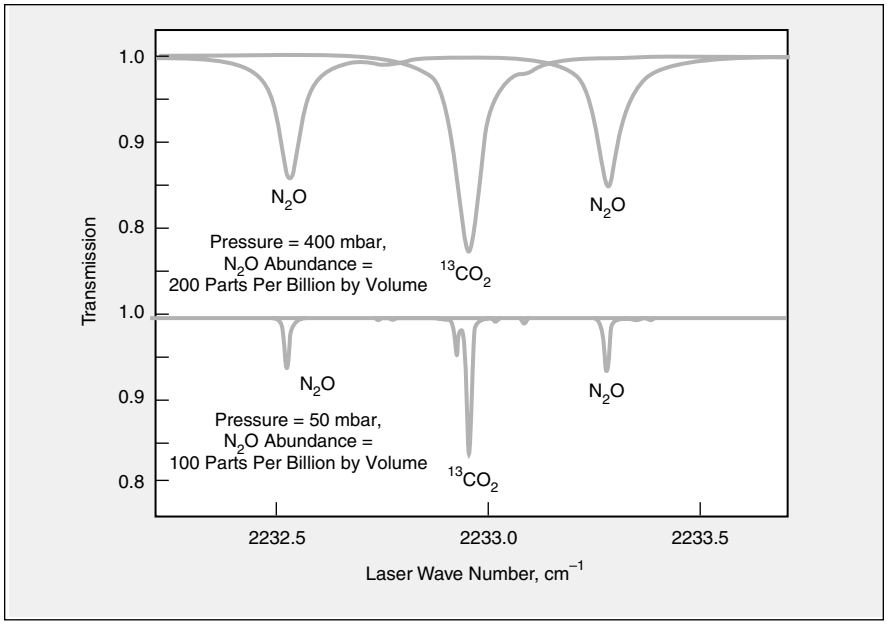


Figure 2. The **Spectral Region Near 1.88 μm** would be appropriate for measurements of water on both Mars and the Earth where suitable near-infrared laser devices would exist.

known and varies slowly and by a small enough amount to be considered constant for calibration in the present context. Hence, absorption-spectral measurements of the concentrations of gases of interest can be normalized to the concentrations of $CO_2$. Because at least one $CO_2$ calibration line is present in every spectral scan of the laser during absorption measurements, the atmospheric $CO_2$ serves continuously as a calibration standard for every measurement point.

Figure 1 depicts simulated spectral transmission measurements in a wavenumber range that contains two absorption lines of $N_2O$ and one of $CO_2$. The simulations were performed for two different upper-atmospheric pressures for an airborne instrument that has a path length of 80 m. The relative abundance of $CO_2$ in air was assumed to be 360 parts per million by volume (approximately its natural level in terrestrial air). In applying the present method to measurements like these, one could average the signals from the two $N_2O$ absorption lines and normalize their magnitudes to that of the $CO_2$ absorption line. Other gases with which this calibration method can be used include $H_2O$, $CH_4$, CO, NO, $NO_2$, HOCl, $C_2H_2$, $NH_3$, $O_3$, and HCN.

One can also take advantage of this method to eliminate an atmospheric-pressure gauge and thereby reduce the mass of the instrument: The atmospheric pressure can be calculated from the temperature, the known relative abundance of $CO_2$, and the concentration of $CO_2$ as measured by spectral absorption.

Natural $CO_2$ levels on Mars provide an ideal calibration standard. Figure 2 shows a second example of the application of this method to Mars atmospheric gas measurements. For sticky gases like $H_2O$, the method is particularly powerful, since water is notoriously difficult to handle at low concentrations in pre-flight calibration procedures.

*This work was done by Chris Webster of Caltech for* **NASA's Jet Propulsion Laboratory**. *For further information, access the Technical Support Package (TSP)* ***free on-line at www.nasatech.com***.
*NPO-30401*

## Laser Ranging Simulation Program

Laser Ranging Simulation Program (LRSP) is a computer program that predicts selected aspects of the performances of a laser altimeter or other laser ranging or remote-sensing systems and is especially applicable to a laser-based system used to map terrain from a distance of several kilometers. Designed to run in a more recent version (5 or higher) of the MATLAB programming language, LRSP exploits the numerical and graphical capabilities of MATLAB. LRSP generates a graphical user interface that includes a pop-up menu that prompts the user for the input of data that determine the performance of a laser ranging system. Examples of input data include duration and energy of the laser pulse, the laser wavelength, the width of the laser

beam, and several parameters that characterize the transmitting and receiving optics, the receiving electronic circuitry, and the optical properties of the atmosphere and the terrain. When the input data have been entered, LRSP computes the signal-to-noise ratio as a function of range, signal and noise currents, and ranging and pointing errors.

*This program was written by Sabino Piazzolla of USC and Hamid Hemmati and David Tratt of Caltech for* **NASA's Jet Propulsion Laboratory**. *For further information, access the Technical Support Package (TSP)* ***free on-line at www.nasatech.com***.

*This software is available for commercial licensing. Please contact Don Hart of the California Institute of Technology at (818) 393-3425. Refer to NPO-30549.*

## Micro-Ball-Lens Optical Switch Driven by SMA Actuator

This could be a prototype of low-loss, mass-producible optical switches.

*NASA's Jet Propulsion Laboratory, Pasadena, California*

The figure is a simplified cross section of a microscopic optical switch that was partially developed at the time of reporting the information for this article. In a fully developed version, light would be coupled from an input optical fiber to one of two side-by-side output optical fibers. The optical connection between the input and the selected output fiber would be made via a microscopic ball lens. Switching of the optical connection from one output fiber to another would be effected by using a pair of thin-film shape-memory-alloy (SMA) actuators to toggle the lens between two resting switch positions.

There are many optical switches — some made of macroscopic parts by conventional fabrication techniques and some that are microfabricated and, hence, belong to the class of microelectromechanical systems (MEMS). Conventionally fabricated optical switches tend to be expensive. MEMS switches can be mass-produced at relatively low cost, but their attractiveness has been diminished by the fact that, heretofore, MEMS switches have usually been found to exhibit high insertion losses. The present switch is intended to serve as a prototype of low-loss MEMS switches. In addition, this is the first reported SMA-based optical switch.

The optical fibers would be held in V grooves in a silicon frame. The lens would have a diameter of 1 μm; it would be held by, and positioned between, the SMA actuators, which would be made of thin films of TiNi alloy. Although the SMA actuators are depicted here as having simple shapes for the sake of clarity of illustration, the real actuators would have complex, partly netlike shapes. With the exception of the lens and the optical fibers, the SMA actuators and other components of the switch would be made by microfabrication techniques. The components would be assembled into a sandwich structure to complete the fabrication of the switch.

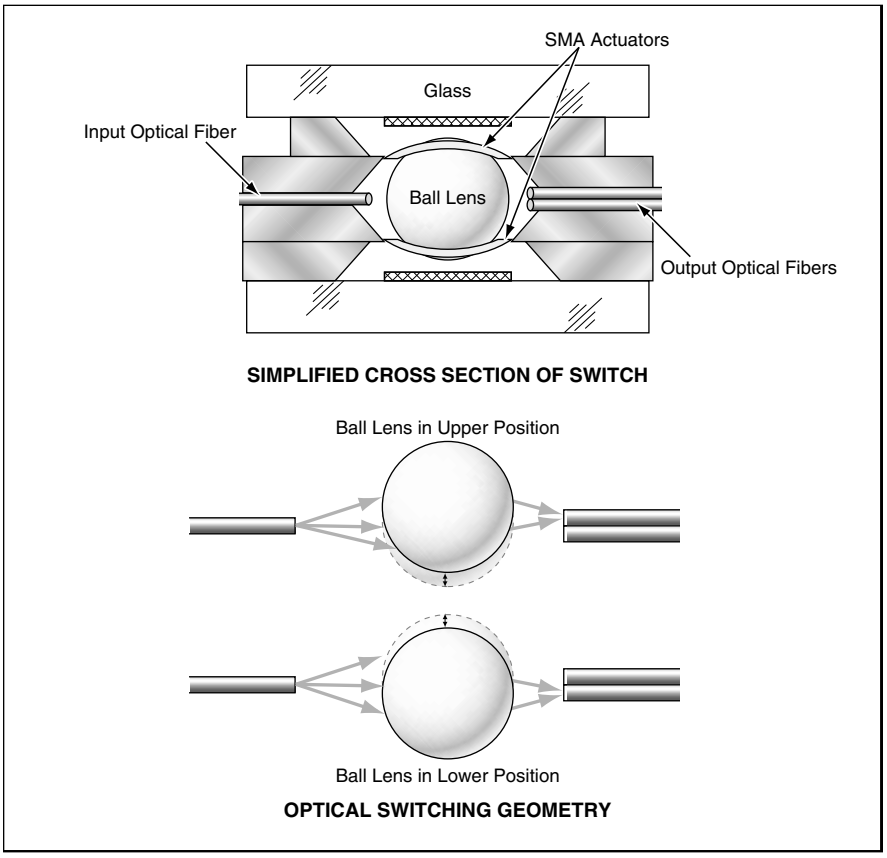


The **SMA Actuators** would move the ball lens between its two resting positions. Light would be coupled to one or the other output optical fiber, depending on which position was selected.

To effect switching, an electric current would be passed through one of the SMA actuators to heat it above its transition temperature, thereby causing it to deform to a different "remembered" shape. The two SMA actuators would be stiff enough that once switching had taken place and the electrical current was turned off, the lens would remain latched in the most recently selected position.

In a test, the partially developed switch exhibited an insertion loss of only –1.9 dB and a switching contrast of 70 dB. One the basis of prior research on SMA actuators and assuming a lens displacement of 125 μm between extreme positions, it has been estimated that the fully developed switch would be capable of operating at a frequency as high as 10 Hz.

*This work was done by Eui-Hyeok Yang of Caltech for* **NASA's Jet Propulsion Laboratory**. *For further information, access the Technical Support Package (TSP)* ***free on-line at www.nasatech.com***.

*NPO-30434*

## Evaluation of Charge Storage and Decay in Spacecraft Insulators

Two reports discuss methods for evaluating the magnitude of electrostatic charging that occurs in spacecraft dielectric materials (in particular, polyimides) during prolonged exposure to radiation in outer space. The reports describe experiments on the electrical resistivities and charge-storage properties of polyimide specimens in a dark, evacuated environment, both before and after 5-megarad exposures to $\gamma$ rays from cobalt-60. The experiments were designed to measure these properties not under standard conditions prescribed for testing dielectrics in air but, rather, under conditions approximating those in the intended spacecraft applications. The results of the experiments showed that the electrical resistivities of the insulations as determined under these conditions are greater, by a factor of roughly a thousand, than those determined under the standard conditions and that the $\gamma$ irradiation reduced resistivities marginally.

*This work was done by Arthur Frederickson and Charles Benson of* **NASA's Jet Propulsion Laboratory** *and James Bockman of Langley Research Center. To obtain copies of the reports, "Processes for Treating Spacecraft Insulators in Order To Prevent Excessive Dielectric Charging" and "Measurement of Charge Storage and Leakage in Polyimides," access the Technical Support Package (TSP)* ***free on-line at www.nasatech.com****.*
*NPO-30482*

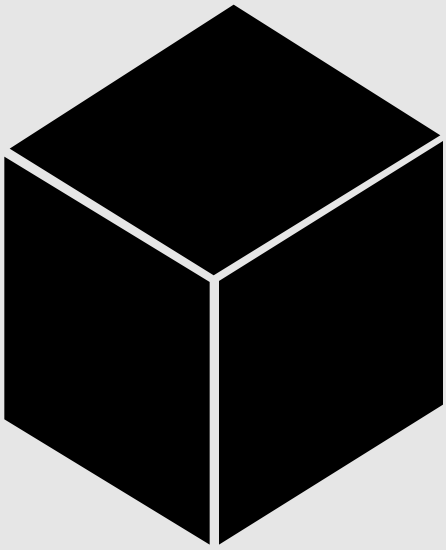

# Materials

## Hardware, Techniques, and Processes


31 Alkaline Capacitors Based on Nitride Nanoparticles
31 Low-EC-Content Electrolytes for Low-Temperature Li-Ion Cells

# Alkaline Capacitors Based on Nitride Nanoparticles

One key to success is an oxygen-free, plasma-assisted nitride-synthesis process.

*John H. Glenn Research Center, Cleveland, Ohio*

High-energy-density alkaline electrochemical capacitors based on electrodes made of transition-metal nitride nanoparticles are undergoing development. Transition-metal nitrides (in particular, $Fe_3N$ and TiN) offer a desirable combination of high electrical conductivity and electrochemical stability in aqueous alkaline electrolytes like KOH. The high energy densities of these capacitors are attributable mainly to their high capacitance densities, which, in turn, are attributable mainly to the large specific surface areas of the electrode nanoparticles. Capacitors of this type could be useful as energy-storage components in such diverse equipment as digital communication systems, implanted medical devices, computers, portable consumer electronic devices, and electric vehicles.

Although the desirable properties of the transition-metal nitrides were known prior to the present development, realization of the inherent electrochemical stability of these materials and of the large specific surface areas and high electrical conductivities needed for high-energy-density capacitors was prevented by side effects of processing:

- Synthesis of these materials involved thermal conversion at temperatures so high (>600 °C) as to cause nucleation of larger particles from smaller ones, with consequent reduction of specific surface areas.
- The nature of the synthesis was such as to yield oxynitrides and oxides in addition to the desired pure nitrides. As a result, electrochemical series resistance (ESR) values were excessive.
- Unlike the nitrides, the oxynitrides and oxides are not sufficiently chemically stable in alkaline electrolytes.

The present development effort follows a multifaceted approach in addressing the aforementioned issues as well as others. In this approach, transition-metal nitride nanoparticles are synthesized at room temperature under conditions that exclude oxygen and thereby prevent the formation of oxynitrides: A synthesis according to this approach involves radio-frequency-plasma-assisted conversion of a nanoparticulate precursor material (e.g., iron acetate, titanium hydride, or titanium chloride) in the presence of anhydrous ammonia gas flowing at a suitable low pressure.

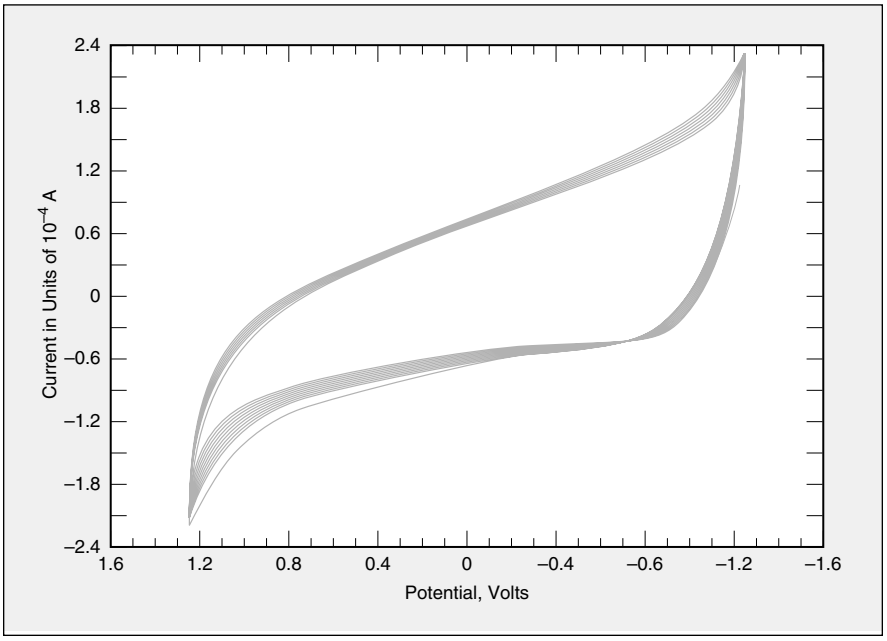


**Cyclic Voltammetry** is a good technique for examining the capacitance, stability, and voltage window of a capacitor. This is a 100-cycle voltammogram, made at a scan rate of 100 mV/s, of a capacitor containing electrodes of nanoparticulate TiN. This plot indicates, among other things, that the electrode material is stable during cycling in the alkaline electrolyte. This cycle exceeds the voltage limits typical of prior capacitors that contain prior carbon or ruthenium oxide electrodes in electrolytes based on sulfuric acid.

Current collectors for the electrodes of the developmental capacitors are made of films of an electrically conductive composite material that consists mostly of TiN nanoparticles in an elastomeric matrix. To ensure highly electrically conductive interfaces with the electrode materials, thin (250-Å thick) coats of TiN can be sputtered onto the surfaces of the current-collector films.

Capacitors designed and fabricated according to the present approach have been characterized in a variety of tests (for example, see figure). A specific capacitance in excess of 150 Farads/gram (F/g) or 800 F/cm$^2$ has been observed. Capacitors of this type, containing both anodes and cathodes made of transition-metal nitride nanoparticles, have withstood potentials >1.75 V. Tests of single-cell and multiple-cell stacks have yielded encouraging results, and significant improvements are expected in future efforts.

*This work was done by Matt Aldissi of Fractal Systems, Inc., for* **Glenn Research Center**. *For further information, access the Technical Support Package (TSP)* ***free online at www.nasatech.com***.

*Inquiries concerning rights for the commercial use of this invention should be addressed to NASA Glenn Research Center, Commercial Technology Office, Attn: Steve Fedor, Mail Stop 4–8, 21000 Brookpark Road, Cleveland, Ohio 44135. Refer to LEW-17083.*

# Low-EC-Content Electrolytes for Low-Temperature Li-Ion Cells

Electrolytes comprising $LiPF_6$ dissolved at a concentration of 1.0 M in three different mixtures of alkyl carbonates have been found well suited for use in rechargeable lithium-ion electrochemical cells at low temperatures. These and other electrolytes have been investigated in continuing research directed toward extending the lower limit of practical operating temperatures of Li-ion cells down to –60 °C. This research at earlier stages was reported in numerous previous *NASA Tech Briefs* articles, the three most recent being "Ethyl Methyl Carbonate as a Cosolvent for Lithium-Ion Cells" (NPO-20605), Vol. 25,

No. 6 (June 2001), page 53; "Alkyl Pyrocarbonate Electrolyte Additives for Li-Ion Cells" (NPO-20775), Vol. 26, No. 5 (May 2002), page 37; and "Fluorinated Alkyl Carbonates as Cosolvents in Li-Ion Cells (NPO-21076), Vol. 26, No. 5 (May 2002), page 38. The present solvent mixtures, in terms of volume proportions of their ingredients, are 1 ethylene carbonate (EC) + 1 diethyl carbonate (DEC) + 1 dimethyl carbonate (DMC) + 3 ethyl methyl carbonate (EMC); 3EC + 3DMC + 14EMC; and 1EC + 1DEC + 1DMC + 4EMC. Relative to similar mixtures reported previously, the present mixtures, which contain smaller proportions of EC, have been found to afford better performance in experimental Li-ion cells at temperatures <–20 °C.

*This work was done by Marshall Smart, Ratnakumar Bugga, and Subbarao Surampudi of Caltech for* **NASA's Jet Propulsion Laboratory**. *For further information, access the Technical Support Package (TSP)* ***free on-line at www.nasatech.com***.

*NPO-30226*

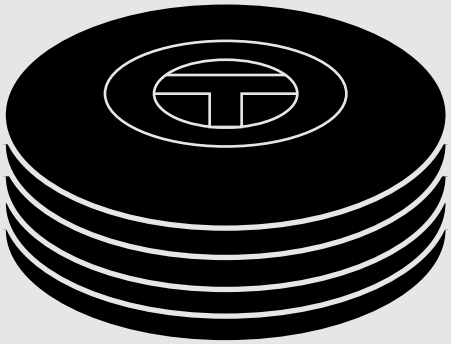

# Computer Programs

## Electronic Systems

35 Software for a GPS-Reflection Remote-Sensing System

## Mathematics and Information Sciences

35 Software for Building Models of 3D Objects via the Internet
35 “Virtual Cockpit Window” for a Windowless Aerospacecraft
36 CLARAty Functional-Layer Software
36 Java Library for Input and Output of Image Data and Metadata
36 Software for Estimating Costs of Testing Rocket Engines

# Electronic Systems

## Software for a GPS-Reflection Remote-Sensing System

A special-purpose software Global Positioning System (GPS) receiver designed for remote sensing with reflected GPS signals is described in "Delay/Doppler-Mapping GPS-Reflection Remote-Sensing System" (NPO-30385), which appears elsewhere in this issue of *NASA Tech Briefs*. The input accepted by this program comprises raw (open-loop) digitized GPS signals sampled at a rate of about 20 MHz. The program processes the data samples to perform the following functions: detection of signals; tracking of phases and delays; mapping of delay, Doppler, and delay/Doppler waveforms; dual-frequency processing; coherent integrations as short as 125 μs; decoding of navigation messages; and precise time tagging of observable quantities. The software can perform these functions on all detectable satellite signals without dead time. Open-loop data collected over water, land, or ice and processed by this software can be further processed to extract geophysical information. Possible examples include mean sea height, wind speed and direction, and significant wave height (for observations over the ocean); bistatic-radar terrain images and measures of soil moisture and biomass (for observations over land); and estimates of ice age, thickness, and surface density (for observations over ice).

*This program was written by Stephen Lowe of Caltech for* **NASA's Jet Propulsion Laboratory**. *For further information, access the Technical Support Package (TSP)* ***free on-line at www.nasatech.com***.

*This software is available for commercial licensing. Please contact Don Hart of the California Institute of Technology at (818) 393-3425. Refer to NPO-30386.*

# Mathematics and Information Sciences

## Software for Building Models of 3D Objects via the Internet

The Virtual EDF Builder (where "EDF" signifies Electronic Development Fixture) is a computer program that facilitates the use of the Internet for building and displaying digital models of three-dimensional (3D) objects that ordinarily comprise assemblies of solid models created previously by use of computer-aided-design (CAD) programs. The Virtual EDF Builder resides on a Unix-based server computer. It is used in conjunction with a commercially available Web-based plug-in viewer program that runs on a client computer. The Virtual EDF Builder acts as a translator between the viewer program and a database stored on the server. The translation function includes the provision of uniform resource locator (URL) links to other Web-based computer systems and databases. The Virtual EDF builder can be used in two ways: (1) If the client computer is Unix-based, then it can assemble a model locally; the computational load is transferred from the server to the client computer. (2) Alternatively, the server can be made to build the model, in which case the server bears the computational load and the results are downloaded to the client computer or workstation upon completion.

*This program was written by Tim Schramer and Jeff Jensen of Boeing North American, Inc., for* **Johnson Space Center**. *For further information, access the Technical Support Package (TSP)* ***free on-line at www.nasatech.com***.
*MSC-22988*

## "Virtual Cockpit Window" for a Windowless Aerospacecraft

A software system processes navigational and sensory information in real time to generate a three-dimensional-appearing image of the external environment for viewing by crewmembers of a windowless aerospacecraft. The design of the particular aerospacecraft (the X-38) is such that the addition of a real transparent cockpit window to the airframe would have resulted in unacceptably large increases in weight and cost.

When exerting manual control, an aircrew needs to see terrain, obstructions, and other features around the aircraft in order to land safely. The X-38 is capable of automated landing, but even when this capability is utilized, the crew still needs to view the external environment: From the very beginning of the United States space program, crews have expressed profound dislike for windowless vehicles. The well-being of an aircrew is considerably promoted by a three-dimensional view of terrain and obstructions. The present software system was developed to satisfy the need for such a view. In conjunction with a computer and display equipment that weigh less than would a real transparent window, this software system thus provides a "virtual cockpit window."

The key problem in the development of this software system was to create a realistic three-dimensional perspective view that is updated in real time. The problem was solved by building upon a pre-existing commercial program — LandForm C3 — that combines the speed of flight-simulator software with the power of geographic-information-system software to generate real-time, three-dimensional-appearing displays of terrain and other features of flight environments. In the development of the present software, the pre-existing program was modified to enable it to utilize real-time information on the position and attitude of the aerospacecraft to generate a view of the external world as it would appear to a person looking out through a window in the aerospacecraft. The development included innovations in realistic horizon-limit modeling, three-dimensional stereographic display, and interfaces for utilization of data from inertial-navigation devices, Global Positioning System receivers, and laser rangefinders. Map and satellite imagery from the National Imagery and Mapping Agency can also be incorporated into displays.

After further development, the present software system and the associated display equipment would be capable of providing a data-enriched view: In addition to terrain and obstacles as they would be seen through a cockpit window, the view could include flight paths, landing zones, aircraft in the vicinity, and unobstructed views of portions of the terrain that might otherwise be hidden from view. Hence, the system could also contribute to safety of flight and landing at night or under conditions of poor visibility.

In recent tests, so precise was the software modeling that during the initial phases of the flight the software running on a monitor beside the video camera produced nearly identical views.

*This work was done by Michael F. Abernathy of Rapid Imaging Software, Inc., for* **Johnson Space Center**. *For fur-*

*ther information, please contact Michael F. Abernathy, Rapid Imaging Software, Inc., 1318 Ridgecrest Place S.E., Albuquerque, NM 87108.*
*MSC-23096*

## CLARAty Functional-Layer Software

Functional-layer software for the Coupled Layer Architecture for Robotics Autonomy (CLARAty) is being developed. [CLARAty was described in "Coupled-Layer Architecture for Advanced Software for Robots" (NPO-21218), *NASA Tech Briefs*, Vol. 26, No. 12 (December 2002), page 48. To recapitulate: CLARAty was proposed to improve the modularity of robotic software while tightening the coupling between planning/execution and control subsystems. Whereas prior robotic software architectures have typically contained three levels, the CLARAty architecture contains two layers: a decision layer and a functional layer.] Just as an operating system provides abstraction from computational hardware, the CLARAty functional-layer software provides for abstraction for the different robotic systems. The functional-layer software establishes interrelated, object-oriented hierarchies that contain active and passive objects that represent the different levels of system abstrations and components. The functional-layer software is decomposed into a set of reusable core components and a set of extended components that adapt the reusable set to specific hardware implementations. The reusable components (a) provide behavior and interface definitions and implementations of basic functionality, (b) provide local executive capabilities, (c) manage local resources, and (d) support state and resource queries by the decision layer. Software for robotic systems can be built by use of these components.

*This software was architected and written by Issa Nesnas, Richard Volpe, Hari Das, Darren Mutz, Richard Petras, and Tara Estlin of Caltech for* **NASA's Jet Propulsion Laboratory**. *For further information, access the Technical Support Package (TSP)* ***free on-line at www.nasatech.com***.

*This software is available for commercial licensing. Please contact Don Hart of the California Institute of Technology at (818) 393-3425. Refer to NPO-30132.*

## Java Library for Input and Output of Image Data and Metadata

A Java-language library supports input and output (I/O) of image data and metadata (label data) in the format of the Video Image Communication and Retrieval (VICAR) image-processing software and in several similar formats, including a subset of the Planetary Data System (PDS) image file format. The library does the following:

- It provides low-level, direct access layer, enabling an application subprogram to read and write specific image files, lines, or pixels, and manipulate metadata directly.
- Two coding/decoding subprograms ("codecs" for short) based on the Java Advanced Imaging (JAI) software provide access to VICAR and PDS images in a file-format-independent manner. The VICAR and PDS codecs enable any program that conforms to the specification of the JAI codec to use VICAR or PDS images automatically, without specific knowledge of the VICAR or PDS format.
- The library also includes Image I/O plug-in subprograms for VICAR and PDS formats. Application programs that conform to the Image I/O specification of Java version 1.4 can utilize any image format for which such a plug-in subprogram exists, without specific knowledge of the format itself. Like the aforementioned codecs, the VICAR and PDS Image I/O plug-in subprograms support reading and writing of metadata.

*This program was written by Robert Deen and Steven Levoe of Caltech for* **NASA's Jet Propulsion Laboratory**. *For further information, access the Technical Support Package (TSP)* ***free on-line at www.nasatech.com***.

*This software is available for commercial licensing. Please contact Don Hart of the California Institute of Technology at (818) 393-3425. Refer to NPO-30470.*

## Software for Estimating Costs of Testing Rocket Engines

A high-level parametric mathematical model for estimating the costs of testing rocket engines and components at Stennis Space Center has been implemented as a Microsoft Excel program that generates multiple spreadsheets. The model and the program are both denoted, simply, the Cost Estimating Model (CEM). The inputs to the CEM are the parameters that describe particular tests, including test types (component or engine test), numbers and duration of tests, thrust levels, and other parameters. The CEM estimates anticipated total project costs for a specific test. Estimates are broken down into testing categories based on a work-breakdown structure and a cost-element structure. A notable historical assumption incorporated into the CEM is that total labor times depend mainly on thrust levels. As a result of a recent modification of the CEM to increase the accuracy of predicted labor times, the dependence of labor time on thrust level is now embodied in third- and fourth-order polynomials.

*This program was developed by Merlon M. Hines of Lockheed Martin Space Operations for* **Stennis Space Center**.

*Inquiries concerning rights for the commercial use of this invention should be addressed to the Intellectual Property Manager, Stennis Space Center [see page 1]. Refer to SSC-00154.*

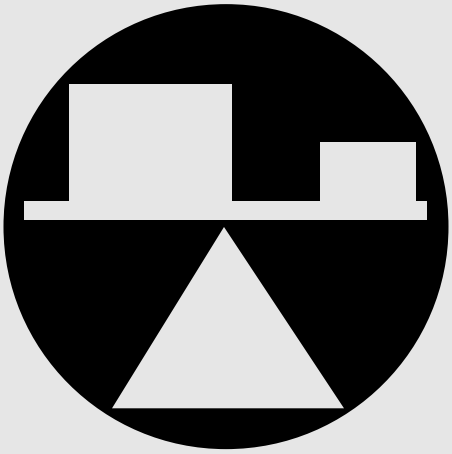

# Mechanics

## Hardware, Techniques, and Processes


39 Energy-Absorbing, Lightweight Wheels

39 Viscoelastic Vibration Dampers for Turbomachine Blades


## Books and Reports


40 Soft Landing of Spacecraft on Energy-Absorbing Self-Deployable Cushions

## Energy-Absorbing, Lightweight Wheels

Efficient structures would absorb impact energies and distribute contact loads.

*NASA's Jet Propulsion Laboratory, Pasadena, California*

Improved energy-absorbing wheels are under development for use on special-purpose vehicles that must traverse rough terrain under conditions (e.g., extreme cold) in which rubber pneumatic tires would fail. The designs of these wheels differ from those of prior non-pneumatic energy-absorbing wheels in ways that result in lighter weights and more effective reduction of stresses generated by ground/wheel contact forces. These wheels could be made of metals and/or composite materials to withstand the expected extreme operating conditions.

As shown in the figure, a wheel according to this concept would include an isogrid tire connected to a hub via spring rods. The isogrid tire would be a stiff, lightweight structure typically made of aluminum. The isogrid aspect of the structure would both impart stiffness and act as a traction surface. The hub would be a thin-walled body of revolution having a simple or compound conical or other shape chosen for structural efficiency. The spring rods would absorb energy and partially isolate the hub and the supported vehicle from impact loads. The general spring-rod configuration shown in the figure was chosen because it would distribute contact and impact loads nearly evenly around the periphery of the hub, thereby helping to protect the hub against damage that would otherwise be caused by large loads concentrated onto small portions of the hub.

The spring rods could be made from any of a variety of materials, depending on the nature of the anticipated loading and the scale of the wheel. (Experiments have shown, for example, that graphite/epoxy spring rods behave in a predictable, repeatable way.) The spring rods would be arranged in a pin/roller beam configuration to load them optimally and prevent the application of thrust loads (that is, loads parallel to the axis of rotation) to the tire. By appropriate sizing of the spring rods and selection of the spring-rod material, the mechanical compliance of the wheel can be tailored over a wide range.

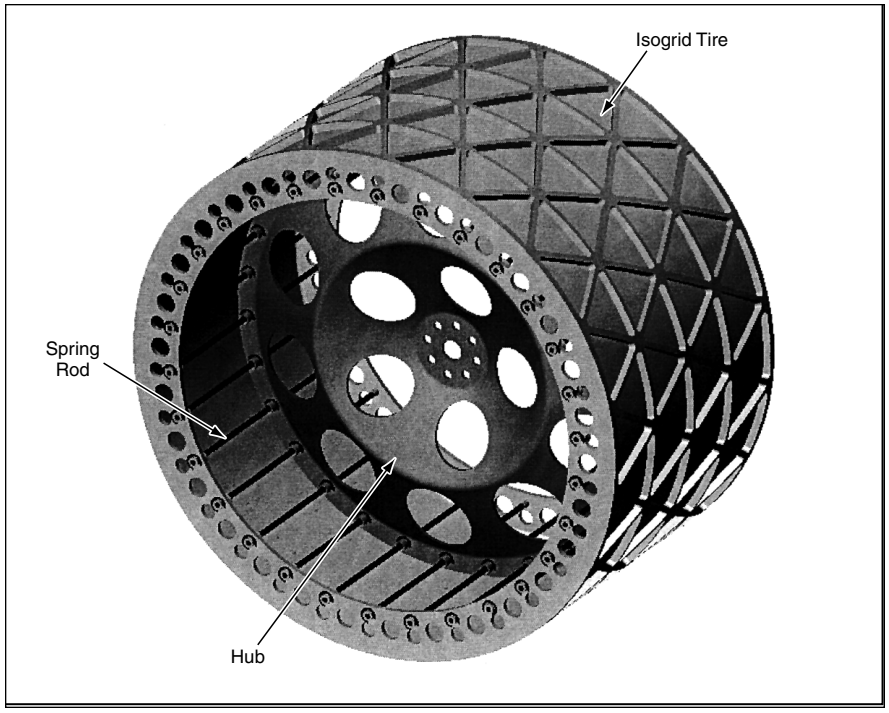


The **Spring Rods** would act as shock absorbers and load distributors between the isogrid tire and the hub.

*This work was done by Peter Waydo of Caltech for* **NASA's Jet Propulsion Laboratory**. *For further information, access the Technical Support Package (TSP)* ***free on-line at www.nasatech.com***.
*NPO-30378*

## Viscoelastic Vibration Dampers for Turbomachine Blades

These dampers can be retrofitted to existing machines.

*Ames Research Center, Moffett Field, California*

Simple viscoelastic dampers have been invented for use on the root attachments of turbomachine blades. These dampers suppress bending- and torsion-mode blade vibrations, which are excited by unsteady aerodynamic forces during operation. In suppressing vibrations, these dampers reduce fatigue (thereby prolonging blade lifetimes) while reducing noise. These dampers can be installed in new turbomachines or in previously constructed turbomachines, without need for structural modifications. Moreover, because these dampers are not exposed to flows, they do not affect the aerodynamic performances of turbomachines.

Figure 1 depicts a basic turbomachine rotor, which includes multiple blades affixed to a hub by means of dovetail root attachments. Prior to mounting of the blades, thin layers of a viscoelastic material are applied to selected areas of the blade roots. Once the blades have been installed in the hub and the rotor is set into rotation, centrifugal force compresses these layers between the mating load-bearing surfaces of the hub and the blade root. The layers of viscoelastic material provide load paths through which the vibration energy of the blade can be dissipated. The viscoelasticity of the material converts mechanical vibration energy into shear strain energy and then from shear strain energy to heat.

Of the viscoelastic materials that have been considered thus far for this application, the one of choice is a commercial polyurethane that is available in tape form, coated on one side with an adhesive that facilitates bonding to blade roots. The thickness of the tape can be chosen to suit the specific application. The typical

thickness of 0.012 in. (≈0.3 mm) is small enough that the tape can fit in the clearance between the mating blade-root and hub surfaces in a typical turbomachine.

In an experiment, a blade was mounted in a test fixture designed to simulate the blade-end conditions that prevail in a turbocompressor. Vibrations were excited in the blade by use of an impact hammer, and damping of the vibrations was measured by use of a dynamic signal analyzer. Tests were performed without and with viscoelastic dampers installed in the dovetail root attachment. The results of the measurements, some of which are presented in Figure 2, show that the viscoelastic dampers greatly increased the rate of damping of vibrations. Accordingly, dynamic stresses on rotor blades were significantly reduced, as shown in Figure 2.

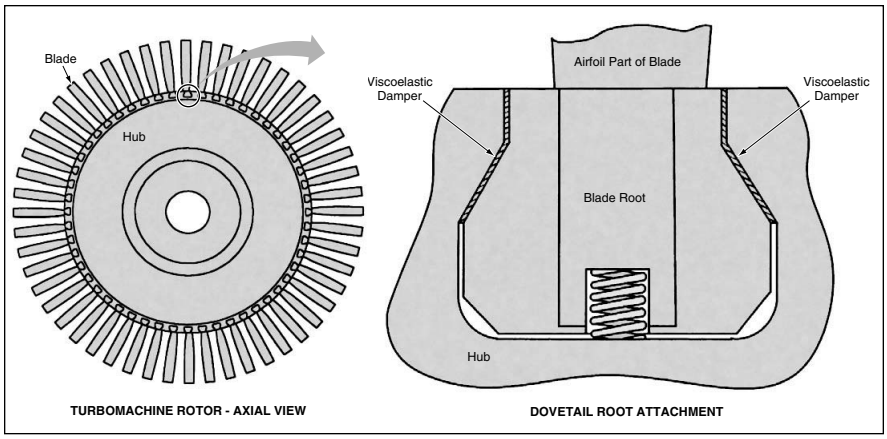


Figure 1. **Thin Layers of Viscoelastic Damping Material** between the blade and hub contact surfaces provide for dissipation of vibrational energy on load paths.

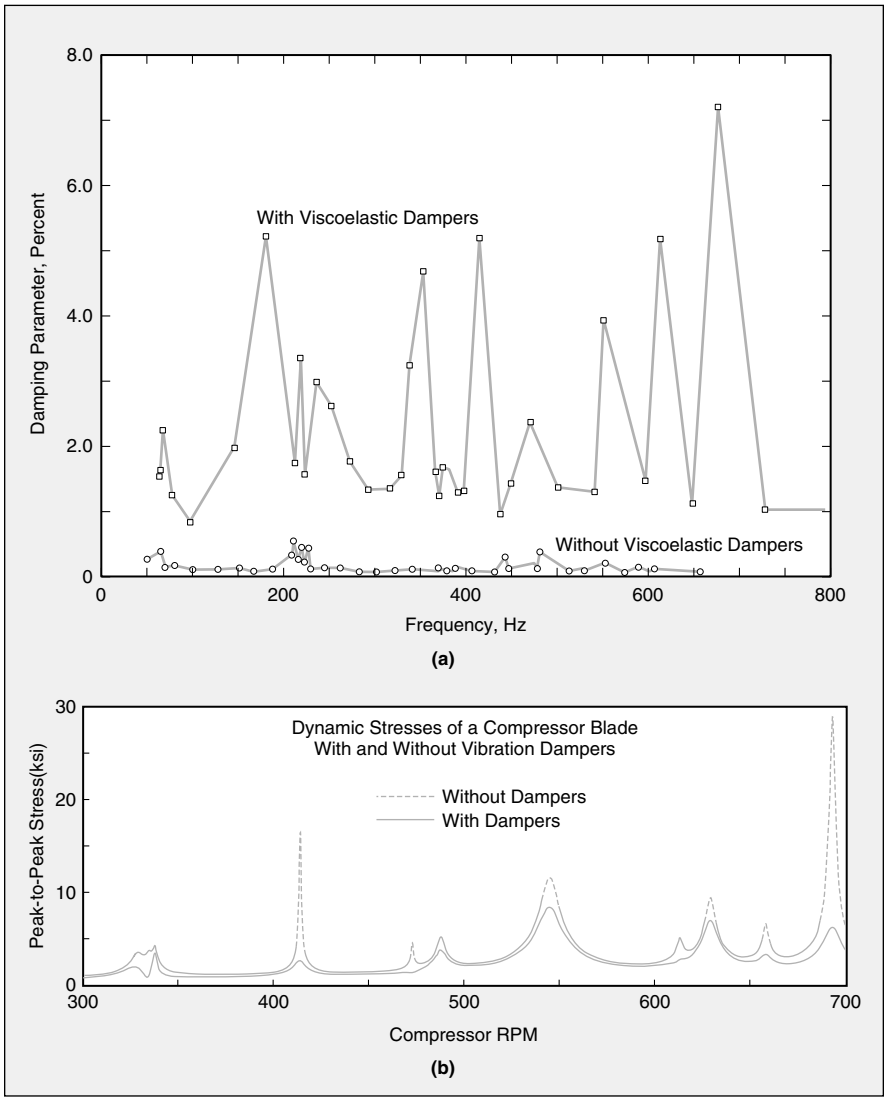


Figure 2. The **Results of the Measurements** have shown that the rate of damping at all frequencies was found to be increased significantly when viscoelastic dampers were installed, as observed in (a). This damping increase results in a significant reduction in operational vibratory stresses of rotor blades in a compressor, as seen in (b).

*This work was done by Nhan Nguyen of* **Ames Research Center**. *For further information, access the Technical Support Package (TSP)* ***free on-line at www.nasatech.com***.

*This invention has been patented by NASA (U.S. Patent No. 6,102,664). Inquiries concerning nonexclusive or exclusive license for its commercial development should be addressed to the Patent Counsel, Ames Research Center, (650) 604-5104. Refer to ARC-14061.*

# Books and Reports

## Soft Landing of Spacecraft on Energy-Absorbing Self-Deployable Cushions

A report proposes the use of cold hibernated elastic memory (CHEM) foam structures to cushion impacts of small (1 to 50 kg) exploratory spacecraft on remote planets. Airbags, which are used on larger (800 to 1,000 kg) spacecraft have been found to (1) be too complex for smaller spacecraft; (2) provide insufficient thermal insulation between spacecraft and ground; (3) bounce on impact, thereby making it difficult to land spacecraft in precisely designated positions; and (4) be too unstable to serve as platforms for scientific observations. A CHEM foam pad according to the proposal would have a glass-transition temperature ($T_g$) well above ambient temperature. It would be compacted, at a temperature above $T_g$, to about a tenth or less of its original volume, then cooled below $T_g$, then installed on a spacecraft without compacting restraints. Upon entry of the spacecraft into a planetary atmosphere, the temperature would rise above $T_g$, causing the pad to expand to its original volume and shape. As the spacecraft decelerated and cooled, the temperature would fall below $T_g$, rigidifying the foam structure. The structure would absorb kinetic energy during ground impact by inelastic crushing, thus protecting the payload from dam-

aging shocks. Thereafter, this pad would serve as a mechanically stable, thermally insulating platform for the landed spacecraft.

*This work was done by Witold Sokolowski and Marc Adams of Caltech for* **NASA's Jet Propulsion Laboratory**. *To obtain a copy of the report, "Novel Precision Soft Lander (PSL)," access the Technical Support Package (TSP)* ***free on-line at www.nasatech.com***.
*NPO-30435*

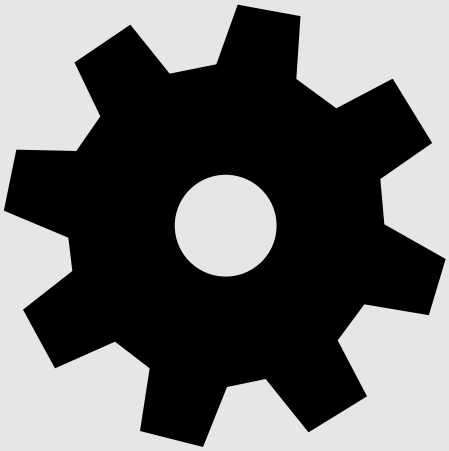

# Machinery

## Hardware, Techniques, and Processes


45 Pneumatically Actuated Miniature Peristaltic Vacuum Pumps
46 Miniature Gas-Turbine Power Generator

# Pneumatically Actuated Miniature Peristaltic Vacuum Pumps

Small, rugged, low-power pumps could be fabricated inexpensively.

*NASA's Jet Propulsion Laboratory, Pasadena, California*

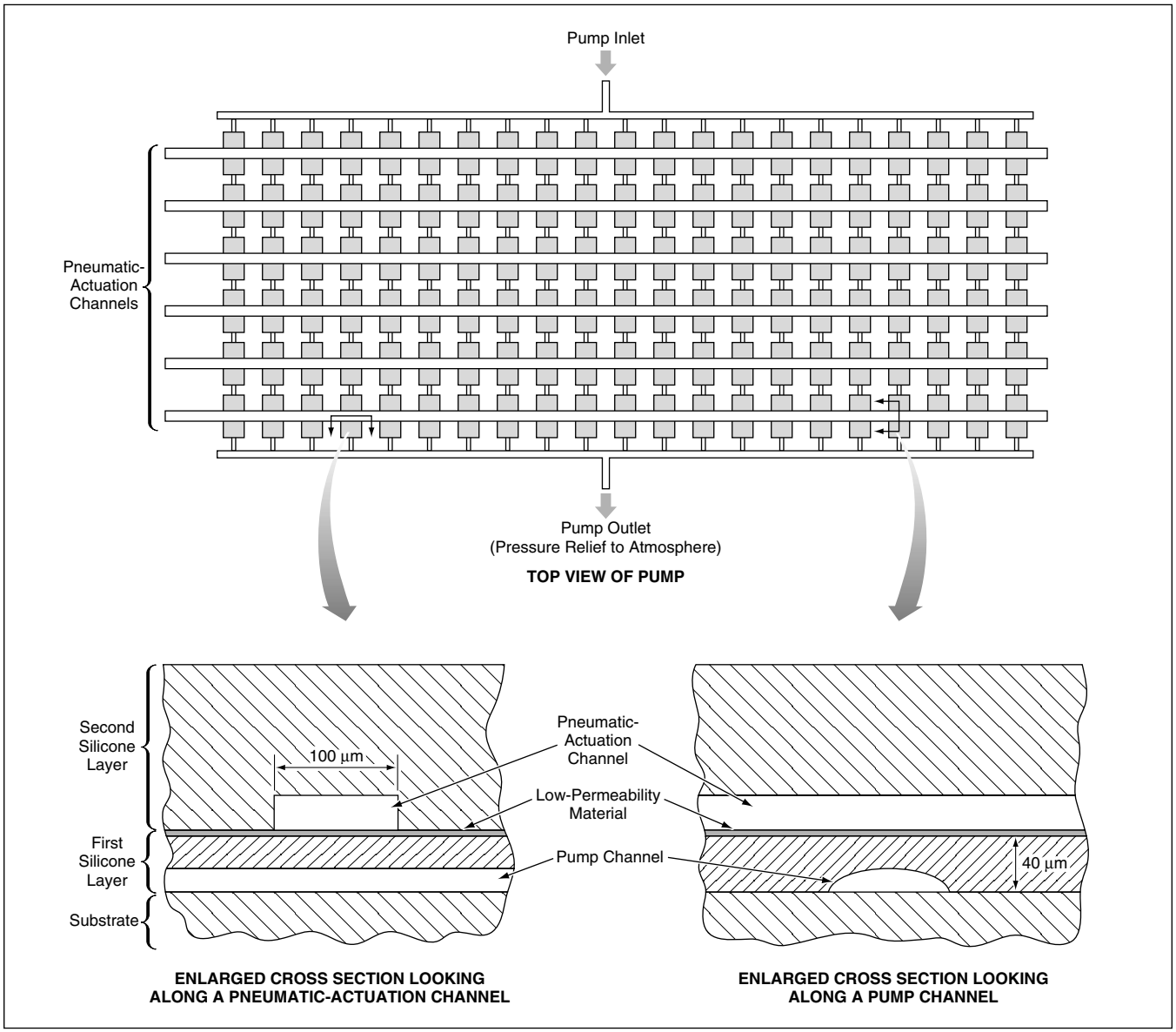


**Pneumatic-Actuation Channels** would be alternately pressurized and depressurized to push down the silicone arches or allow them to spring back up, respectively. This action would create waves of opening and closing, equivalent to peristalsis, that would move gases along the pump channels. The dimensions shown here are exemplary, not exclusive.

Pneumatically actuated miniature peristaltic vacuum pumps have been proposed for incorporation into advanced miniature versions of scientific instruments that depend on vacuum for proper operation. These pumps are expected to be capable of reaching vacuum-side pressures in the torr to millitorr range (from ≈133 down to ≈0.13 Pa). Vacuum pumps that operate in this range are often denoted roughing pumps. In comparison with previously available roughing pumps, these pumps are expected to be an order of magnitude less massive and less power-hungry. In addition, they would be extremely robust, and would operate with little or no maintenance and without need for oil or other lubricants. Portable mass spectrometers are typical examples of instruments that could incorporate the proposed pumps. In addition, the proposed pumps could be used as roughing pumps in general laboratory applications in which low pumping rates could be tolerated.

The proposed pumps could be designed and fabricated in conventionally machined and micromachined versions. A typical micromachined version (see figure) would include a rigid glass, metal, or plastic substrate and two layers of silicone rubber. The bottom silicone layer would contain shallow pump channels covered by silicone arches that could be pushed down pneumatically to block the channels. The bottom silicone layer would be covered with a thin layer of material with very low gas permeability, and would be bonded to the substrate everywhere except in the channel areas. The top silicone layer would be attached to the bottom silicone layer and would contain pneumatic-actuation channels that would lie crosswise to the pump channels. This ver-

sion is said to be micromachined because the two silicone layers containing the channels would be fabricated by casting silicone rubber on micromachined silicon molds.

The pneumatic-actuation channels would be alternately connected to a compressed gas and (depending on pump design) either to atmospheric pressure or to a partial vacuum source. The design would be such that the higher pneumatic pressure would be sufficient to push the silicone arches down onto the substrates, blocking the channels. Thus, by connecting pneumatic-actuation channels to the two pneumatic sources in spatial and temporal alternation, waves of opening and closing, equivalent to peristalsis, could be made to move along the pump channels.

A pump according to this concept could be manufactured inexpensively. Pneumatic sources (compressors and partial vacuum sources) similar those needed for actuation are commercially available; they typically have masses of ≈100 g and power demands of the order of several W. In a design-optimization effort, it should be possible to reduce masses and power demands below even these low levels and to integrate pneumatic sources along with the proposed pumps into miniature units with overall dimensions of no more than a few centimeters per side.

*This work was done by Sabrina Feldman, Jason Feldman, and Danielle Svehla of Caltech for* **NASA's Jet Propulsion Laboratory**. *For further information, access the Technical Support Package (TSP)* ***free on-line at www.nasatech.com***.
*NPO-30165*

## Miniature Gas-Turbine Power Generator

Energy density would greatly exceed that of a typical battery system.

*NASA's Jet Propulsion Laboratory, Pasadena, California*

A proposed microelectromechanical system (MEMS) containing a closed-Brayton-cycle turbine would serve as a prototype of electric-power generators for special applications in which high energy densities are required and in which, heretofore, batteries have been used. The system would have a volume of about 6 $cm^3$ and would operate with a thermal efficiency >30 percent, generating up to 50 W of electrical power. The energy density of the proposed system would be about 10 times that of the best battery-based systems now available, and, as such, would be comparable to that of a fuel cell.

The working gas for the turbine would be Xe containing small quantities of $CO_2$, $O_2$, and $H_2O$ as gaseous lubricants. The gas would be contained in an enclosed circulation system, within which the pressure would typically range between 5 and 50 atm (between 0.5 and 5 MPa). The heat for the Brayton cycle could be supplied by any of a number of sources, including a solar concentrator or a combustor burning a hydrocarbon or other fuel. The system would include novel heat-transfer and heat-management components. The turbine would be connected to an electric power generator/starter motor.

The system would include a main rotor shaft with gas bearings; the bearing surfaces would be made of a ceramic material coated with nanocrystalline diamond. The shaft could withstand speed of 400,000 rpm or perhaps more, with bearing-wear rates less than $10^{-4}\times$ those of silicon bearings and 0.05 to 0.1× those of SiC bearings, and with a coefficient of friction about 0.1× that of Si or SiC bearings. The components of the system would be fabricated by a combination of (1) three-dimensional x-ray lithography and (2) highly precise injection molding of diamond-compatible metals and ceramic materials. The materials and fabrication techniques would be suitable for mass production.

The disadvantages of the proposed system are that unlike a battery-based system, it could generate a perceptible amount of sound, and, if it were to burn fuel, then it would also generate exhaust, similarly to other combustion-based power sources.

*This work was done by Dean Wiberg, Stephen Vargo, Victor White, and Kirill Shcheglov of Caltech and Phillip Muntz of the University of Southern California for* **NASA's Jet Propulsion Laboratory**. *For further information, access the Technical Support Package (TSP)* ***free on-line at www.nasatech.com***.
*NPO-20933*

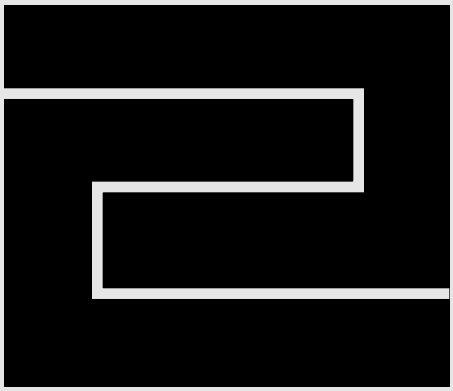

# Fabrication Technology

## Hardware, Techniques, and Processes


49 Pressure-Sensor Assembly Technique
49 Wafer-Level Membrane-Transfer Process for Fabricating MEMS
51 A Reactive-Ion Etch for Patterning Piezoelectric Thin Film

# Pressure-Sensor Assembly Technique

An essential underfilling step can be performed without compromising a diaphragm.

*John H. Glenn Research Center, Cleveland, Ohio*

Nielsen Engineering & Research (NEAR) recently developed an ultrathin data acquisition system for use in turbomachinery testing at NASA Glenn Research Center. This system integrates a microelectromechanical-systems- (MEMS-) based absolute pressure sensor [0 to 50 psia (0 to 345 kPa)], temperature sensor, signal-conditioning application-specific integrated circuit (ASIC), microprocessor, and digital memory into a package which is roughly 2.8 in. (7.1 cm) long by 0.75 in. (1.9 cm) wide. Each of these components is flip-chip attached to a thin, flexible circuit board and subsequently ground and polished to achieve a total system thickness of 0.006 in. (0.15 mm). Because this instrument is so thin, it can be quickly adhered to any surface of interest where data can be collected without disrupting the flow being investigated.

One issue in the development of the ultrathin data acquisition system was how to attach the MEMS pressure sensor to the circuit board in a manner which allowed the sensor's diaphragm to communicate with the ambient fluid while providing enough support for the chip to survive the grinding and polishing operations. The technique, developed by NEAR and Jabil Technology Services Group (San Jose, CA), is described below. In the approach developed, the sensor is attached to the specially designed circuit board, see Figure 1, using a modified flip-chip technique. The circular diaphragm on the left side of the sensor is used to actively measure the ambient pressure, while the diaphragm on the right is used to compensate for changes in output due to temperature variations. The circuit board is fabricated with an access hole through it so that when the completed system is installed onto a wind tunnel model (chip side down), the active diaphragm is exposed to the environment. After the sensor is flip-chip attached to the circuit board, the die is underfilled to support the chip during the subsequent grinding and polishing operations. To prevent this underfill material from getting onto the sensor's diaphragms, the circuit board is fabricated with two 25-micrometer-tall polymer rings, sized so that the diaphragms fit inside the rings once the chip is attached.

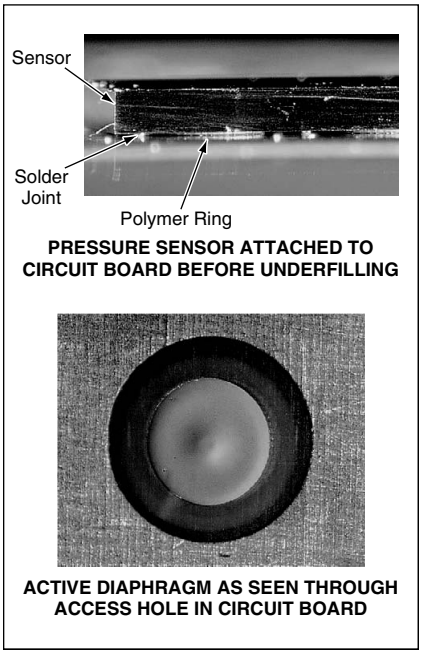


Figure 2. **Critical Components** of the instrument are shown here at two different stages in the assembly process.

During the reflow operation, the solder bumps on the chip melt and spread out over the circuit board's bond pads thus pulling the chip down until its face rests on the top of the two polymer rings. A series of experiments were conducted to determine the optimal size for the solder bumps so that the sensor chip seated properly on the rings while adequate solder joints were formed between the chip and the circuit board. A side view showing the chip and circuit board after soldering, but before underfilling, is provided in the upper part of Figure 2.

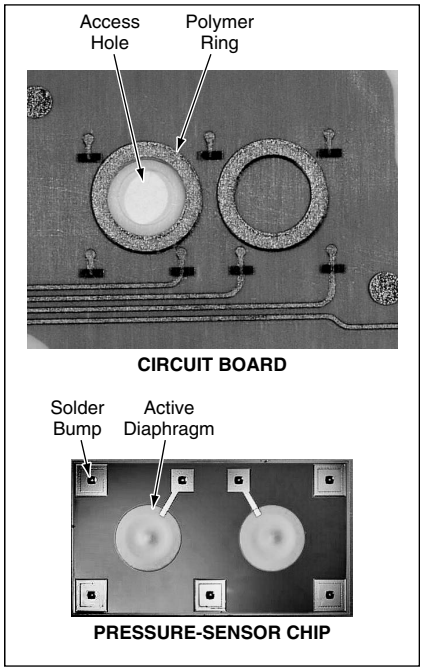


Figure 1. The **Pressure-Sensor Chip and Circuit Board** are shown here as they appear before they are put together by use of a modified flip-chip technique.

With the sensor resting on the polymer rings, the chip can be underfilled without the risk of contaminating the diaphragms. The active diaphragm is shown in the lower part of Figure 2, as seen through the access hole in the circuit board after the chip was attached and underfilled. The technique described provides a means for securely attaching and underfilling a MEMS-based pressure sensor to a circuit board while allowing the diaphragm access to the ambient fluid.

*This work was done by Daniel A. Pruzan of Nielsen Engineering and Research for* **Glenn Research Center**. *Refer to LEW-17212.*

# Wafer-Level Membrane-Transfer Process for Fabricating MEMS

This process is well suited for structures fabricated on dissimilar substrates.

*NASA's Jet Propulsion Laboratory, Pasadena, California*

A process for transferring an entire wafer-level micromachined silicon structure for mating with and bonding to another such structure has been devised. This process is intended especially for use in wafer-level integration of microelectromechanical systems (MEMS) that have been fabricated on dissimilar substrates.

Unlike in some older membrane-transfer processes, there is no use of wax or epoxy during transfer. In this process, the substrate of a wafer-level structure to be transferred serves as a carrier, and is etched away once the transfer has been completed. Another important feature of this process is that two

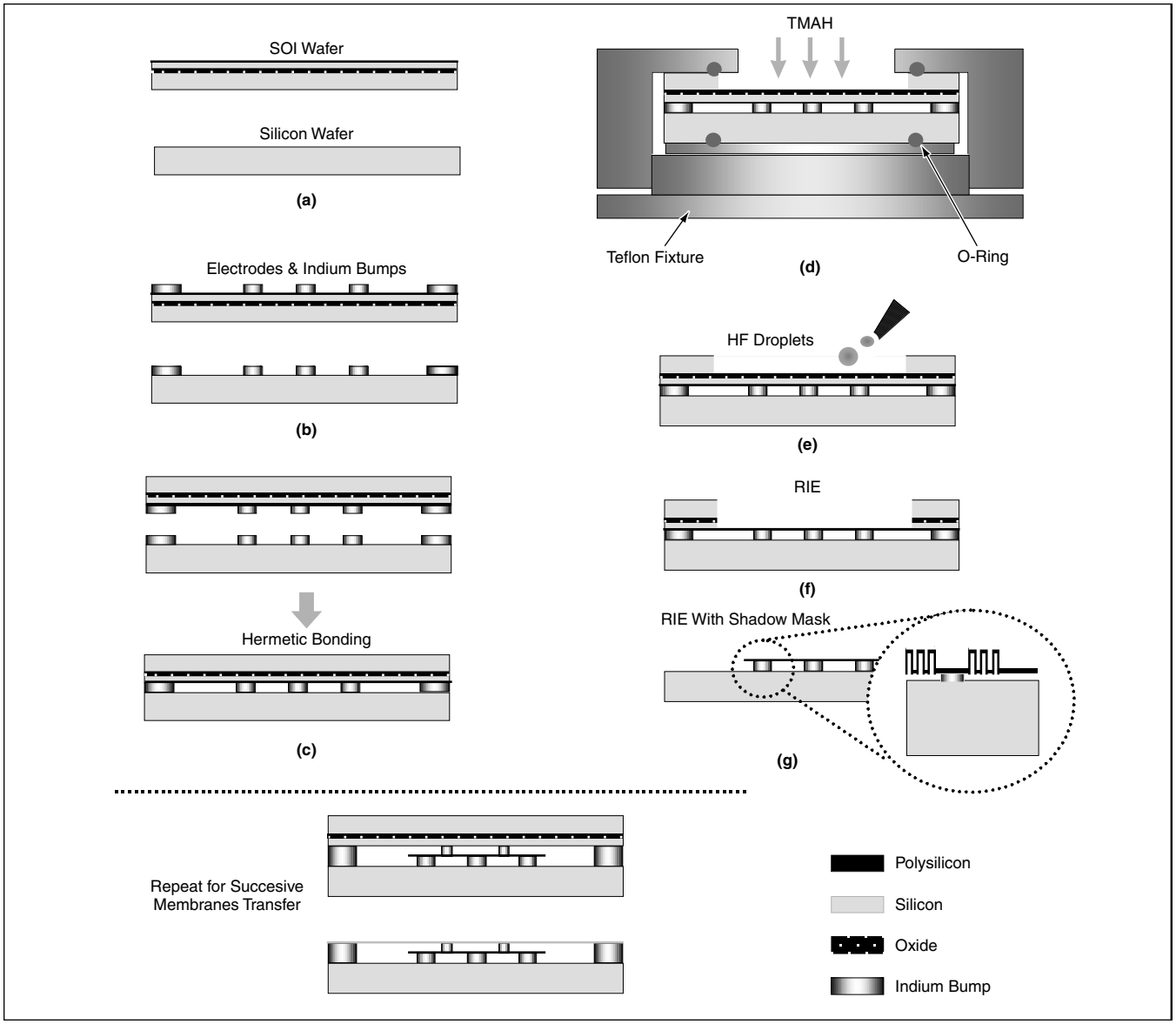


Figure 1. An **Outline of the Process** shows the key steps.

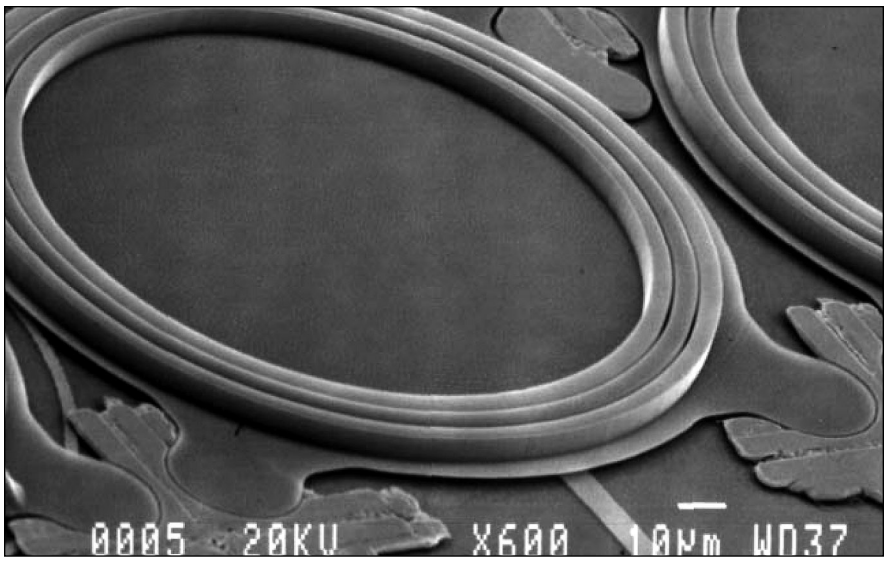


Figure 2. A **Corrugated Polysilicon Membrane**, only 1 µm thick, was transferred onto a silicon substrate to form an array of electrostatic actuators. The actuators were found to function as intended.

wafer-level structures to be integrated with each other are indium-bump-bonded together; this is advantageous in that it produces less (in comparison with other bonding techniques) stress during bonding of structures formed on two dissimilar wafers. Moreover, unlike in some older membrane-transfer processes, there is no incidental release of HF from the final structure — an advantage when indium, aluminum, or another soft metal is used for bonding.

This process was demonstrated by applying it to the joining of (1) a corrugated polycrystalline silicon (polysilicon) membrane that had been fabricated by patterning and etching on a silicon-on-insulator (SOI) wafer with (2) a silicon substrate. A 1-µm thick corrugated polysilicon membrane has been transferred onto an electrode wafer to show the feasibility of the proposed technique. The transferred membrane with underlying

electrodes constitutes an electrostatic actuator array. An SOI wafer and a silicon wafer (see Figure 1) are used as the carrier and electrode wafers, respectively. After oxidation, both wafers are patterned and etched to define a corrugation profile and electrode array, respectively. The polysilicon layer is deposited on the SOI wafer. The carrier wafer is bonded to the electrode wafer by using evaporated indium bumps. The piston pressure of 4 kPa is applied at 156 °C in a vacuum chamber to provide hermetic sealing. The substrate of the SOI wafer is etched in a 25 weight percent TMAH bath at 80 °C. The exposed buried oxide is then removed by using 49 percent HF droplets after an oxygen plasma ashing. The SOI top silicon layer is etched away by using an $SF_6$ plasma to define the corrugation profile, followed by the HF droplet etching of the remaining oxide. The $SF_6$ plasma with a shadow mask selectively etches the polysilicon membrane, if the transferred membrane structure needs to be patterned. Electrostatic actuators with various electrode gaps have been fabricated by this transfer technique. The gap between the transferred membrane and electrode substrate is very uniform (±0.1 μm across a wafer diameter of 100 mm, provided by optimizing the bonding control). Figure 2 depicts the finished product.

*This work was done by Eui-Hyeok Yang and Dean Wiberg of Caltech for* **NASA's Jet Propulsion Laboratory**. *For further information, access the Technical Support Package (TSP)* ***free on-line at www.nasatech.com***.

*In accordance with Public Law 96-517, the contractor has elected to retain title to this invention. Inquiries concerning rights for its commercial use should be addressed to*

*Technology Reporting Office*
*JPL*
*Mail Stop 249-103*
*4800 Oak Grove Drive*
*Pasadena, CA 91109*
*(818) 354-2240*

*Refer to NPO-21088, volume and number of this* NASA Tech Briefs *issue, and the page number.*

# A Reactive-Ion Etch for Patterning Piezoelectric Thin Film

Gaseous mixtures $BCl_3$ and $Cl_2$ are highly selective for etching $PbZr_{1-x}Ti_xO_3$ films.

*NASA's Jet Propulsion Laboratory, Pasadena, California*

Reactive-ion etching (RIE) under conditions described below has been found to be a suitable means for patterning piezoelectric thin films made from such materials as $PbZr_{1-x}Ti_xO_3$ or $Ba_xSr_{1-x}TiO_3$. In the original application for which this particular RIE process was developed, $PbZr_{1-x}Ti_xO_3$ films 0.5 μm thick are to be sandwiched between Pt electrode layers 0.1 μm thick and Ir electrode layers 0.1 μm thick to form piezoelectric capacitor structures. Such structures are typical of piezoelectric actuators in advanced microelectromechanical systems now under development or planned to be developed in the near future.

RIE of $PbZr_{1-x}Ti_xO_3$ is usually considered to involve two major subprocesses: an ion-assisted-etching reaction, and a sputtering subprocess that removes reactive byproducts. RIE is favored over other etching techniques because it offers a potential for a high degree of anisotropy, high-resolution pattern definition, and good process control. However, conventional RIE is not ideal for patterning $PbZr_{1-x}Ti_xO_3$ films at a thickness as great as that in the original intended application. In order to realize the potential benefits mentioned above, it is necessary to optimize process conditions — in particular, the composition of the etching gas and the values of such other process parameters as radio-frequency power, gas pressure, gas-flow rate, and duration of the process. Guidelines for determining optimum conditions can be obtained from experimental determination of etch rates as functions of these parameters.

Etch-gas mixtures of $BCl_3$ and $Cl_2$, some also including Ar, have been found to offer a high degree of selectivity as needed for patterning of $PbZr_{1-x}Ti_xO_3$ films on top of Ir electrode layers in thin-film capacitor structures. The selectivity is characterized by a ratio of ≈10:1 (rate of etching $PbZr_{1-x}Ti_xO_3$ ÷ rate of etching Ir and $IrO_x$). At the time of reporting the information for this article, several experiments on RIE in $BCl_3$ and $Cl_2$ (and sometimes Ar) had demonstrated the 10:1 selectivity ratio, and further experiments to enhance understanding and obtain further guidance for optimizing process conditions were planned.

*This work was done by Eui-Hyeok Yang and Larry Wild of Caltech for* **NASA's Jet Propulsion Laboratory**. *For further information, access the Technical Support Package (TSP)* ***free on-line at www.nasatech.com***.

*In accordance with Public Law 96-517, the contractor has elected to retain title to this invention. Inquiries concerning rights for its commercial use should be addressed to*

*Intellectual Assets Office*
*JPL*
*Mail Stop 202-233*
*4800 Oak Grove Drive*
*Pasadena, CA 91109*
*(818) 354-2240*
*E-mail: ipgroup@jpl.nasa.gov*

*Refer to NPO-30349, volume and number of this* NASA Tech Briefs *issue, and the page number.*

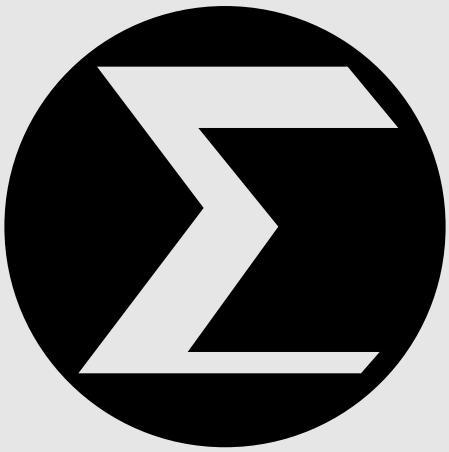

# Mathematics and Information Sciences

## Hardware, Techniques, and Processes


55 Wavelet-Based Real-Time Diagnosis of Complex Systems
56 Quantum Search in Hilbert Space
56 Analytic Method for Computing Instrument Pointing Jitter

# Wavelet-Based Real-Time Diagnosis of Complex Systems

Changes in hardware and software can be simultaneously examined for signs of loss of control.

*NASA's Jet Propulsion Laboratory, Pasadena. California*

A new method of robust, autonomous real-time diagnosis of a time-varying complex system (e.g., a spacecraft, an advanced aircraft, or a process-control system) is presented here. It is based upon the characterization and comparison of (1) the execution of software, as reported by discrete data, and (2) data from sensors that monitor the physical state of the system, such as performance sensors or similar quantitative time-varying measurements. By taking account of the relationship between execution of, and the responses to, software commands, this method satisfies a key requirement for robust autonomous diagnosis, namely, ensuring that control is maintained and followed.

Such monitoring of control software requires that estimates of the state of the system, as represented within the control software itself, are representative of the physical behavior of the system. In this method, data from sensors and discrete command data are analyzed simultaneously and compared to determine their correlation. If the sensed physical state of the system differs from the software estimate (see figure) or if the system fails to perform a transition as commanded by software, or such a transition occurs without the associated command, the system has experienced a control fault. This method provides a means of detecting such divergent behavior and automatically generating an appropriate warning.

The method is general enough to detect changes in a variety of systems, characterized by cycle times ranging from milliseconds to months or beyond. Detection of changes is accomplished using a wavelet decomposition, which is scalable to arbitrary temporal characteristics and sensitive to changes in any derivative. Wavelet decomposition itself is computationally efficient and is widely used in signal conditioning and image compression. Our method applies a similar approach to time-varying signals and performs an extraction and characterization of significant events, which serves as detector and classifier of commanded responses and anomalies based upon their temporal and spatial characteristics. This method is fundamentally superior to traditional fault monitoring, which relies upon thresholds set upon absolute sensor data, derivatives, and the like. The wavelet filter also offers the advantage of adaptability to nearly any signal.

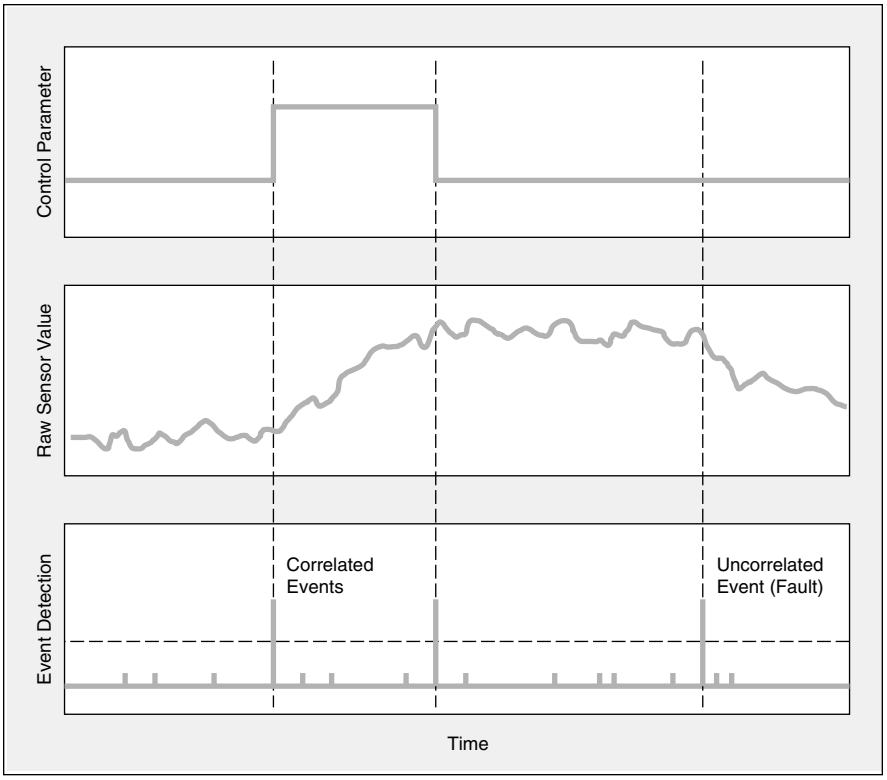


In this **Simple Example,** events detected from a paired control signal and sensor signal are initially temporally correlated, but they do not show correlation as expected. The uncorrelated event is detected by this method and signifies the occurrence of a fault.

The method is implemented by applying the scalable algorithm directly to raw or preconditioned signal data. The algorithm resolves generic transitions and characterizes them in a low-order dimensional representation, according to the scaling and perfect-reconstruction capabilities of the wavelet decomposition. This algorithm is applied alongside a logical difference operator acting upon preselected discrete data signal representative of software control. Selection of these signal pairs can be performed manually using expert knowledge, or through other elements of BEAM (Beacon-Based Exception Analysis for Multimissions), which is described in "Software for Autonomous Diagnosis of Complex Systems" (NPO-20827), *NASA Tech Briefs*, Vol. 26, No. 9 (September 2002), page 32). Events in the two streams are detected and compared according to temporal index, confirming consistent system/software execution or revealing the presence of anomalous behavior.

The final output of the algorithm includes a simple flag indicating nominal or faulty operation. Information on the time of fault onset and parameters characterizing the fault are also provided. Such information can be directed to the system control or further analyzed as part of the complete BEAM framework. This method is sensitive to both hard failures and incipient faults, including degradation and sensor failure, in addition to monitoring control and response.

*This work was done by Sandeep Gulati and Ryan Mackey of Caltech for* **NASA's Jet Propulsion Laboratory**. *For further information, access the Technical Support Package (TSP)* ***free on-line at www.nasatech.com***.

*NPO-20830*

## Quantum Search in Hilbert Space

A large database would be searched in one quantum computing operation.

*NASA's Jet Propulsion Laboratory, Pasadena, California*

A proposed quantum-computing algorithm would perform a search for an item of information in a database stored in a Hilbert-space memory structure. The algorithm is intended to make it possible to search relatively quickly through a large database under conditions in which available computing resources would otherwise be considered inadequate to perform such a task.

The algorithm would apply, more specifically, to a relational database in which information would be stored in a set of $N$ complex orthonormal vectors, each of $N$ dimensions (where $N$ can be exponentially large). Each vector would constitute one row of a unitary matrix, from which one would derive the Hamiltonian operator (and hence the evolutionary operator) of a quantum system. In other words, all the stored information would be mapped onto a unitary operator acting on a quantum state that would represent the item of information to be retrieved. Then one could exploit quantum parallelism: one could pose all search queries simultaneously by performing a quantum measurement on the system. In so doing, one would effectively solve the search problem in one computational step.

One could exploit the direct- and inner-product decomposability of the unitary matrix to make the dimensionality of the memory space exponentially large by use of only linear resources. However, inasmuch as the necessary preprocessing (the mapping of the stored information into a Hilbert space) could be exponentially expensive, the proposed algorithm would likely be most beneficial in applications in which the resources available for preprocessing were much greater than those available for searching.

*This work was done by Michail Zak of Caltech for* **NASA's Jet Propulsion Laboratory**. *For further information, access the Technical Support Package (TSP)* ***free on-line at www.nasatech.com***.
*NPO-30193*

## Analytic Method for Computing Instrument Pointing Jitter

Jitter can be computed more efficiently.

*NASA's Jet Propulsion Laboratory, Pasadena, California*

A new method of calculating the root-mean-square (rms) pointing jitter of a scientific instrument (e.g., a camera, radar antenna, or telescope) is introduced based on a state-space concept. In comparison with the prior method of calculating the rms pointing jitter, the present method involves significantly less computation.

The rms pointing jitter of an instrument (the square root of the jitter variance shown in the figure) is an important physical quantity which impacts the design of the instrument, its actuators, controls, sensory components, and sensor-output-sampling circuitry. Using the Sirlin, San Martin, and Lucke definition of pointing jitter, the prior method of computing the rms pointing jitter involves a frequency-domain integral of a rational polynomial multiplied by a transcendental weighting function, necessitating the use of numerical-integration techniques. In practice, numerical integration complicates the problem of calculating the rms pointing error. In contrast, the state-space method provides exact analytic expressions that can be evaluated without numerical integration.

The theoretical foundation of the state-space method includes a representation of the pointing process as a stationary process generated by a state-space model driven by white noise. The state-space formulation results in the replacement of the aforementioned weighted frequency integral with the calculation of a matrix exponential. Additional simplifications may be possible in certain applications by taking

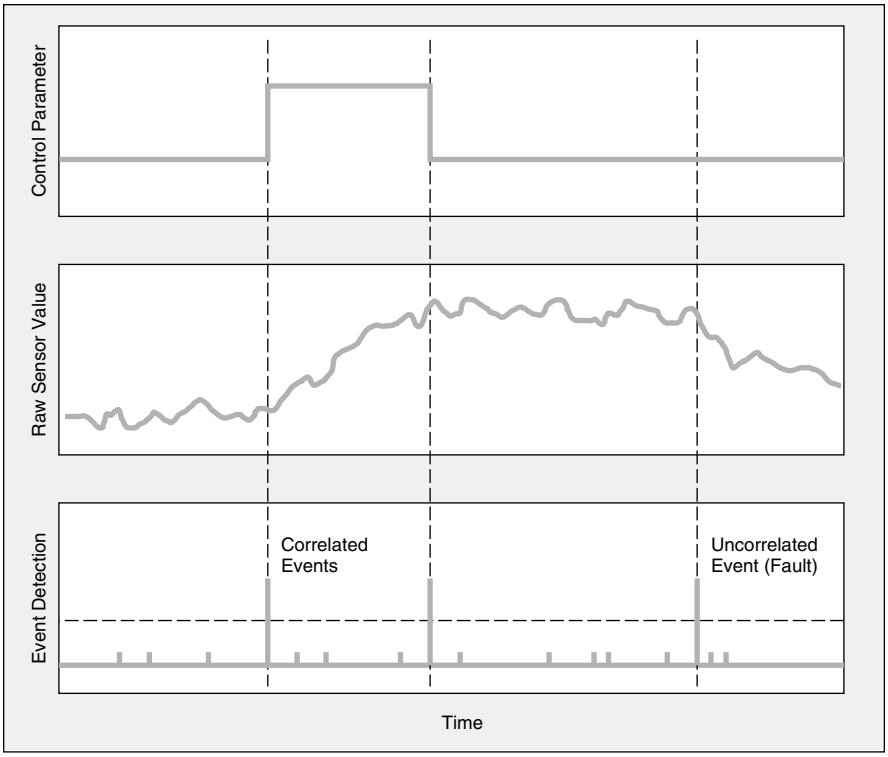


**Instantaneous and Statistical Quantities** are used to characterize the pointing of an instrument (that is, rotation of the instrument about an axis). The quantities shown here pertain to a pointing process $y(t)$ at instant of time $t$ during an observation interval (window) of duration $T$ that starts at time $\tau$, $E[]$ is an expectation operator denoting the ensemble average of the bracketed term, $n(t)$ is a zero-mean white-noise process, and $Cov[]$ is an ensemble-average covariance operator.

advantage of well-known matrix exponential expressions and/or inverse Laplace transform relationships. Two useful examples of such simplifications are given in the report. In addition to simplifying the calculations, the closed-form expressions provide insight into physical mechanisms of jitter.

*This work was done by David Bayard of Caltech for* **NASA's Jet Propulsion Laboratory**. *For further information, access the Technical Support Package (TSP)* ***free on-line at www.nasatech.com.*** *NPO-30525*

# Life Sciences

## Hardware, Techniques, and Processes

61 Semiselective Optoelectronic Sensors for Monitoring Microbes

# Semiselective Optoelectronic Sensors for Monitoring Microbes

These real-time sensors distinguish among classes (not individual species) of microbes.

*Lyndon B. Johnson Space Center, Houston, Texas*

Sensor systems are under development for use in real-time detection and quantitation of microbes in water without need for sampling. These systems include arrays of optical sensors; miniature, portable electronic data-acquisition circuits; and optoelectronic interfaces between the sensor arrays and data-acquisition circuits. These systems are intended for original use in long-term, in-line monitoring of waterborne micro-organisms in water-reclamation systems aboard future spacecraft. They could also be adapted to similar terrestrial uses with respect to municipal water supplies, stored drinking water, and swimming water; for detecting low-level biological contamination in biotechnological, semiconductor, and pharmaceutical process streams; and in verifying the safety of foods and beverages. In addition, they could be adapted to monitoring of airborne microbes and of surfaces (e.g., to detect and/or quantitate biofilms).

The designs of the sensors in these systems are based partly on those of sensors developed previously for monitoring airborne biological materials. The designs exploit molecular-recognition and fluorescence-spectroscopy techniques, such that in the presence of micro-organisms of interest, fluorescence signals change and the changes can be measured.

These systems are characterized as semiselective because they respond to classes of micro-organisms and can be used to discriminate among the classes. This semiselectivity is a major aspect of the design: It is important to distinguish between (1) the principle of detection and quantitation of classes of micro-organisms by use of these sensors and (2) the principle of detection and quantitation of individual microbiological species by means of prior immunodiagnostic and/or molecular-biology techniques. Detection of classes (in contradistinction to species) is particularly valuable when the exact nature of a contaminant is unknown.

Feasibility was demonstrated by fabricating sensor systems that were then demonstrated to be capable of detecting bacteria with rapid response and high sensitivity, to discriminate between gram positive and gram negative bacteria, and to detect fungi in water. In one of the experiments, a capability of real-time, cumulative response to bacteria in a flow system was demonstrated.

An important part of the development effort thus far has addressed the issue of designing and building sensors and sensing membranes for extended use in aqueous flow systems. Another major issue is that of calibration: A capability for calibration has been demonstrated. It has also been shown that calibration of sensors at low concentrations is a potential source of quantitation error, though not of detection error.

*This work was done by Mary Beth Tabacco, Han Chuang, Laura Taylor, and Jaimie Russo of Echo Technologies, Inc., for* **Johnson Space Center**.

*In accordance with Public Law 96-517, the contractor has elected to retain title to this invention. Inquiries concerning rights for its commercial use should be addressed to*

*Echo Technologies, Inc.*
*451 D Street*
*Boston, MA 02210*

*Refer to MSC-23237, volume and number of this* NASA Tech Briefs *issue, and the page number.*

National Aeronautics and
Space Administration